

A modified adaptive improved mapped WENO method

Ruo Li^a, Wei Zhong^{b,c,*}

^a*CAPT, LMAM and School of Mathematical Sciences, Peking University, Beijing 100871, China*

^b*School of Mathematical Sciences, Peking University, Beijing 100871, China*

^c*Northwest Institute of Nuclear Technology, Xi'an 710024, China*

Abstract

We propose several adaptive control functions and a smoothing approximation of the signum function, and apply them to design mapping functions used to construct new mapped weighted essentially non-oscillatory (WENO) schemes. Our method extends the formulation of the mapping functions used in the WENO-IM(k, A) methods developed in the last years. The new method admits a more extensive permitted range of the parameters in the mapping functions, that it enjoys some mathematical advantages in achieving optimal convergence rates. Improved numerical results are obtained for one-dimensional linear advection cases, especially over long output times. Numerical solutions of the 1D Euler equations with the Sod's shock tube problem, the Shu-Osher shock-entropy wave interaction problem and the Woodward-Colella blastwave problem are compared with results in references. Quite satisfied performances using the new method are demonstrated in the simulation of two severe problems as the Titarev-Toro shock-entropy wave interaction problem and the 123 problem.

Keywords: WENO schemes, Adaptive mapping functions, Hyperbolic conservation laws

1. Introduction

In recent decades, the essentially non-oscillatory (ENO) schemes [13, 15, 14, 12] and weighted ENO (WENO) schemes [22, 23, 20, 18, 21] have been developed quite successfully to solve the hyperbolic conservation laws in the form

$$\frac{\partial \mathbf{u}}{\partial t} + \sum_{\alpha=1}^d \frac{\partial \mathbf{f}_{\alpha}(\mathbf{u})}{\partial x_{\alpha}} = 0, \quad x_{\alpha} \in \mathbb{R}, t > 0, \quad (1)$$

where $\mathbf{u} = (u_1, u_2, \dots, u_m) \in \mathbb{R}^m$ are the conserved variables and $\mathbf{f}_{\alpha} : \mathbb{R}^m \rightarrow \mathbb{R}^m$, $\alpha = 1, 2, \dots, d$ are the Cartesian components of flux. Within the general framework (referred as WENO-JS below) of smoothness indicators and non-linear weights proposed by Jiang and Shu [18], many successful works have improved the accuracy and efficiency of WENO schemes [16, 8, 7, 2, 3, 17, 5, 1].

Henrick et al. [16] found that the fifth-order WENO-JS scheme is only third-order accurate at critical points of order $n_{cp} = 1$ in the smooth regions, where n_{cp} denotes the order of the critical point; e.g., $n_{cp} = 1$ corresponds to $f' = 0, f'' \neq 0$ and $n_{cp} = 2$ corresponds to $f' = 0, f'' = 0, f''' \neq 0$, etc. They derived necessary and sufficient conditions [16] on the weights for optimality of the order and developed the WENO-M method [16] to achieve the optimal order of accuracy by introducing a mapping function to the original weights of WENO-JS. Feng et al. found that, when the mapping function in [16] is used for solving the problems with discontinuities, it may amplify the effect from the non-smooth stencils, thereby causing a potential loss of accuracy near discontinuities [7]. In order to address this issue, they devised the WENO-PM k scheme [7] by proposing a piecewise polynomial mapping function with two additional requirements, that is, $g'(0) = 0$ and $g'(1) = 0$ ($g(x)$ denotes the mapping function), to the original criteria in [16]. Also, these two additional requirements were considered to be very important to decrease

*Corresponding author

Email addresses: rli@math.pku.edu.cn (Ruo Li), zhongwei2016@pku.edu.cn (Wei Zhong)

the effect from the non-smooth stencils [29] and were used in the construction of the WENO-RM($mn0$) scheme [29]. Similarly, requirements $g'(0) = 1$ and $g'(1) = 1$ were employed when the WENO-PPM n ($n = 4, 5, 6$) [19] schemes were constructed. Although the mapping function in WENO-PM k scheme decreases the effect from the non-smooth stencils, it is not smooth enough [7] because it is only piecewise continuous. Furthermore, WENO-PM k scheme may generate the oscillations near discontinuities [29]. Recently, Feng et al. [8] proposed a new family of mapping functions to improve the WENO-M method, referred as the WENO-IM(k, A) method depended on two parameters k and A . The WENO-IM(k, A) method with proper parameters can achieve optimal order of accuracy near critical points for any $(2r - 1)$ th-order WENO scheme and provide better numerical solutions [8] with less dissipation and higher resolution for the fifth-order WENO method than WENO-JS, WENO-M and WENO-Z [2]. However, it is required that k to be an even integer [8] in WENO-IM(k, A), which may prevent one from finding the best mapped WENO method of the WENO-IM(k, A) method. Moreover, it is easy to verify that the mapping function in WENO-IM(k, A) could not satisfy the requirements, namely $g'(0) = 0$ or $g'(0) = 1$, to decrease the effect from the non-smooth stencils, which may lead to the numerical solution with non-physical oscillations near the discontinuity [29].

In this paper, by introducing several adaptive control functions and using a smoothing approximation of the signum function, we propose a group of new mapping functions, which satisfies: first, it has a very similar form to the mapping function of WENO-IM(k, A) but the permitted range of parameter k is extended from positive even integers to any positive integer; second, it keeps $g'(0) = 1$ and $g'(1) = 1$ so that it can decrease the effect from the non-smooth stencils; third, it is smooth enough; fourth, when applied to the fifth-order method, it does not produce non-physical oscillations near the discontinuities in long time simulations as WENO-PM k does [8, 29]. We prove that the optimal order of accuracy at or near the critical points in smooth regions can be recovered by using the new mapping functions. Extensive numerical experiments show that, our new method performs satisfactory for those benchmark problems in the references. Meanwhile, some of our new schemes have comparable advantages in calculating the Woodward-Colella interacting blast waves problem [30]. And particularly, our new schemes perform very well in some severe test problem, like the the Titarev-Toro shock-entropy wave interaction problem [25, 27, 26] and the 123 problem [6, 28, 4]. The 123 problem is useful in assessing the performance of numerical methods for low density flows [28] and many conservative schemes may fail to simulate it [6] by predicting non-physical states with negative density or internal energy.

The rest of this paper is organized as follows. In Section 2, we give a brief description of the finite volume method and the procedures of WENO-JS [18], WENO-M [16], WENO-PM k [7] and WENO-IM(k, A) [8] to clarify our major concern. In Section 3, the details on how we construct the modified adaptive improved mapped WENO method, referred as WENO-MAIM i later on, are presented. In Section 4, some numerical experiments are presented to compare the performances of different WENO methods. Finally, some concluding remarks are made in Section 5.

2. Description of finite volume WENO methods

In this section, we first review the implementation of the finite volume method [28] and then recall the essentials of the classic WENO-JS scheme proposed in [18], along with the mapped version WENO-M introduced in [16] and the WENO-PM k and WENO-IM(k, A) schemes introduced in [7] and [8], respectively.

2.1. Finite volume method

Considering the one-dimensional scalar case, we rewrite Eq.(1) as follows,

$$\frac{\partial u}{\partial t} + \frac{\partial f(u)}{\partial x} = 0, \quad x \in [x_l, x_r], t > 0. \quad (2)$$

For simplicity, we assume that the computational domain is distributed into smaller uniform cells $I_j = [x_{j-1/2}, x_{j+1/2}]$, where $\Delta x = x_{j+1/2} - x_{j-1/2}$ is the mesh width, $x_{j\pm 1/2} = x_j \pm \frac{\Delta x}{2}$ are the interfaces of I_j and $x_j = \frac{1}{2}(x_{j+1/2} + x_{j-1/2})$ are the cell centers. After some simple mathematical manipulations, we can approximate Eq.(2) by the following finite volume conservative formulation

$$\frac{d\bar{u}_j(t)}{dt} \approx -\frac{1}{\Delta x}(\hat{f}_{j+1/2} - \hat{f}_{j-1/2}),$$

where $\bar{u}_j(t)$ is the numerical approximation to the cell average $\bar{u}_j = \frac{1}{\Delta x} \int_{x_{j-1/2}}^{x_{j+1/2}} u(\xi, t) d\xi$ and the numerical flux $\hat{f}_{j+1/2}$ is a function of $u(x, t)$ at the cell boundary, namely, $u_{j+1/2}^\pm$, defined by

$$\hat{f}_{j+1/2} = \hat{f}(u_{j+1/2}^-, u_{j+1/2}^+), \quad (3)$$

where $\hat{f}(u^-, u^+)$ is a monotone numerical flux. In this paper, we take the global Lax-Friedrichs flux $\hat{f}(a, b) = \frac{1}{2}[f(a) + f(b) - \alpha(b - a)]$, where $\alpha = \max_u |f'(u)|$ is a constant and the maximum is taken over the whole range of u . In Eq.(3), $u_{j+1/2}^\pm$ can be obtained from some kind of WENO reconstruction, which is detailed in the following subsections. For the systems of conservation laws, a local characteristic decomposition is used in the reconstruction, and [18, 21] are referred to for more details.

2.2. The classic WENO-JS reconstruction

The three 3rd-order approximations of $u(x_{j+1/2}, t)$ in the left-biased substencils $S_3^s = \{x_{j+s-2}, x_{j+s-1}, x_{j+s}\}$ are defined as

$$u_{j+1/2}^{s,-} = \sum_{i=0}^2 c_{si} \bar{u}_{j+s-i}, \quad s = 0, 1, 2, \quad (4)$$

where c_{si} are Lagrangian interpolation coefficients (see [21, 18]) that depend on parameter s but not on the values of \bar{u}_j . Explicitly, we have

$$\begin{aligned} u_{j+1/2}^{0,-} &= \frac{1}{3}\bar{u}_{j-2} - \frac{7}{6}\bar{u}_{j-1} + \frac{11}{6}\bar{u}_j, \\ u_{j+1/2}^{1,-} &= -\frac{1}{6}\bar{u}_{j-1} + \frac{5}{6}\bar{u}_j + \frac{1}{3}\bar{u}_{j+1}, \\ u_{j+1/2}^{2,-} &= \frac{1}{3}\bar{u}_j + \frac{5}{6}\bar{u}_{j+1} - \frac{1}{6}\bar{u}_{j+2}. \end{aligned}$$

The fifth-degree polynomial approximation $u_{j+1/2}^- = u(x_{j+1/2}, t) + O(\Delta x^5)$ is built via the convex combination of the interpolated values $u_{j+1/2}^{s,-}$ in Eq.(4)

$$u_{j+1/2}^- = \sum_{s=0}^2 \omega_s u_{j+1/2}^{s,-},$$

where ω_s are called nonlinear weights taking the smoothness of the solution into consideration. In the classic WENO-JS reconstruction, they are computed as

$$\omega_s^{\text{JS}} = \frac{\alpha_s^{\text{JS}}}{\sum_{l=0}^2 \alpha_l^{\text{JS}}}, \quad \alpha_s^{\text{JS}} = \frac{d_s}{(\epsilon + \beta_s)^2}. \quad (5)$$

Here, ϵ is a small positive number that is introduced to prevent the denominator becoming zero, and d_s are the optimal weights satisfying $\sum_{s=0}^2 d_s u_{j+1/2}^{s,-} = u(x_{j+1/2}, t) + O(\Delta x^5)$. For fifth-order WENO schemes, they are given by $d_0 = 0.1, d_1 = 0.6, d_2 = 0.3$. The parameters β_s are called smoothness indicators, which are defined as follows

$$\begin{aligned} \beta_0 &= \frac{13}{12}(\bar{u}_{j-2} - 2\bar{u}_{j-1} + \bar{u}_j)^2 + \frac{1}{4}(\bar{u}_{j-2} - 4\bar{u}_{j-1} + 3\bar{u}_j)^2, \\ \beta_1 &= \frac{13}{12}(\bar{u}_{j-1} - 2\bar{u}_j + \bar{u}_{j+1})^2 + \frac{1}{4}(\bar{u}_{j-1} - \bar{u}_{j+1})^2, \\ \beta_2 &= \frac{13}{12}(\bar{u}_j - 2\bar{u}_{j+1} + \bar{u}_{j+2})^2 + \frac{1}{4}(3\bar{u}_j - 4\bar{u}_{j+1} + \bar{u}_{j+2})^2. \end{aligned}$$

In smooth regions without critical points, the WENO-JS scheme gives the fifth-order accuracy. However, near critical points, its order of accuracy decreases to third order or even less. For more details, we refer to [16, 18].

2.3. The mapped WENO-M reconstruction

A mapping function of the nonlinear weights ω was constructed by Henrick et al. [16] to correct the deficiency of the WENO-JS method mentioned above. The mapping function is written as

$$(g^M)_s(\omega) = \frac{\omega(d_s + (d_s)^2 - 3d_s\omega + \omega^2)}{(d_s)^2 + (1 - 2d_s)\omega}, \quad \omega \in [0, 1], \quad (6)$$

It is easy to verify that the mapping function $(g^M)_s(\omega)$ is a monotonically increasing function in $[0, 1]$ with finite slopes that satisfies the following properties.

Lemma 1. *If the mapping function is defined by Eq.(6), it satisfies:*

- C1. $0 \leq (g^M)_s(\omega) \leq 1, (g^M)_s(0) = 0, (g^M)_s(1) = 1;$
- C2. $(g^M)_s(\omega) \approx 0$ if $\omega \approx 0; (g^M)_s(\omega) \approx 1$ if $\omega \approx 1;$
- C3. $(g^M)_s(d_s) = d_s, (g^M)'_s(d_s) = (g^M)''_s(d_s) = 0.$

Mapping function Eq.(6) is employed to obtain the mapped weights as

$$\omega_s^M = \frac{\alpha_s^M}{\sum_{l=0}^2 \alpha_l^M}, \alpha_s^M = (g^M)_s(\omega_s^{JS}),$$

In smooth regions, the WENO-M scheme gives the fifth-order accuracy even near the first-order critical points where the first derivative vanishes, and [16] can be referred to for more details.

2.4. The piecewise polynomial WENO-PMk reconstructions

To overcome the potential loss of accuracy near the discontinuities or the parts with sharp gradients [7] caused by the mapping function $(g^M)_s(\omega)$, Feng et al. add two requirements, $g'_i(0) = g'_i(1) = 0$, to the original criteria by Henrick et al. [16]. And then they give the new mapped weights as follows

$$\omega_s^{PM} = \frac{\alpha_s^{PM}}{\sum_{l=0}^2 \alpha_l^{PM}}, \alpha_s^{PM} = (g^{PM})_s(\omega_s^{JS}),$$

where $(g^{PM})_s(\omega)$ is a piecewise polynomial function taking the form [7]

$$(g^{PM})_s(\omega) = C_1(\omega - d_s)^{k+1}(\omega + C_2) + d_s, \quad k \geq 2, \quad (7)$$

where C_1, C_2 are constants and given by

$$(C_1, C_2) = \begin{cases} \left((-1)^k \frac{k+1}{d_s^{k+1}}, \frac{d_s}{k+1} \right), & \text{if } 0 \leq \omega \leq d_s, \\ \left(-\frac{k+1}{(1-d_s)^{k+1}}, \frac{d_s - (k+2)}{k+1} \right), & \text{if } d_s < \omega \leq 1. \end{cases}$$

Lemma 2. *If the mapping function is defined by Eq.(7), it satisfies:*

- C1. $(g^{PM})'_s(\omega) \geq 0, \omega \in [0, 1];$
- C2. $(g^{PM})'_s(0) = 0, (g^{PM})'_s(d_s) = d_s, (g^{PM})'_s(1) = 1;$
- C3. $(g^{PM})'_s(d_s) = \dots = (g^{PM})^{(k)}_s(d_s) = 0;$
- C4. $(g^{PM})'_s(0) = (g^{PM})'_s(1) = 0.$

2.5. The improved mapped WENO-IM(k, A) reconstructions

An improved mapped WENO-IM(k, A) reconstruction was proposed by Feng et al. [8]. By rewriting the mapping function Eq.(6), they obtained a new type of mapping function of the form

$$(g^{\text{IM}})_s(\omega; k, A) = d_s + \frac{(\omega - d_s)^{k+1} A}{(\omega - d_s)^k A + \omega(1 - \omega)}, \quad A > 0, k = 2n, n \in \mathbb{N}^+, \quad (8)$$

and the corresponding improved mapped weights are given by

$$\omega_s^{\text{IM}} = \frac{\alpha_s^{\text{IM}}}{\sum_{l=0}^2 \alpha_l^{\text{IM}}}, \quad \alpha_s^{\text{IM}} = (g^{\text{IM}})_s(\omega_s^{\text{JS}}; k, A).$$

It is trivial to show that the mapping function Eq.(6) belongs to the family of the improved mapping functions Eq.(8) by choosing $A = 1, k = 2$. Moreover, the improved mapping functions Eq.(8) have the following properties.

Lemma 3. *If the mapping functions are defined by Eq.(8), they satisfy:*

- C1. $(g^{\text{IM}})'_s(\omega; k, A) \geq 0, \omega \in [0, 1]$;
- C2. $(g^{\text{IM}})'_s(0; k, A) = 0, (g^{\text{IM}})_s(d_s; k, A) = d_s, (g^{\text{IM}})_s(1; k, A) = 1$;
- C3. $(g^{\text{IM}})'_s(d_s; k, A) = \dots = (g^{\text{IM}})^{(k)}_s(d_s; k, A) = 0, (g^{\text{IM}})^{(k+1)}_s(d_s; k, A) \neq 0$.

The detailed proof of Lemma 3 can be found in the statement on page 456 in [8].

2.6. Time discretization

Commonly, WENO schemes are employed in a method of lines (MOL) approach, where one discretizes space while leaving time continuous. Then, following this approach, we turn the PDE Eq.(2) into a large number of coupled ODEs, resulting in the system of equations

$$\frac{d\bar{u}_j(t)}{dt} = \mathcal{L}(u_j), \quad (9)$$

where $\mathcal{L}(u_j)$ is the result of the application of the WENO scheme and is defined as

$$\mathcal{L}(u_j) := -\frac{1}{\Delta x}(\hat{f}_{j+1/2} - \hat{f}_{j-1/2}).$$

Throughout this paper, we solve the ODEs system Eq.(9) using the explicit, third-order, TVD, Runge-Kutta method [22, 10, 11] as follows

$$\begin{aligned} u^{(1)} &= u^n + \Delta t \mathcal{L}(u^n), \\ u^{(2)} &= \frac{3}{4}u^n + \frac{1}{4}u^{(1)} + \frac{1}{4}\Delta t \mathcal{L}(u^{(1)}), \\ u^{n+1} &= \frac{1}{3}u^n + \frac{2}{3}\Delta t \mathcal{L}(u^{(2)}), \end{aligned}$$

where $u^{(1)}$ and $u^{(2)}$ are the intermediate stages, u^n is the value of u at time level $t^n = n\Delta t$, and Δt is the time step satisfying some proper CFL condition.

3. The modified adaptive improved mapped WENO reconstructions

3.1. The adaptive control functions

In order to obtain the property $g'(0) = g'(1) = 1$, we introduce two adaptive control functions, namely $f_{i,s}^{\text{Ada0}}$ and $f_{i,s}^{\text{Ada1}}$, in our new mapping functions which will be proposed in a later subsection. For $f_{i,s}^{\text{Ada0}}$ and $f_{i,s}^{\text{Ada1}}$, the following two requirements need to be satisfied: (1) if ω tends to 0 or 1, the product $\omega^{f_{i,s}^{\text{Ada0}}}(1 - \omega)^{f_{i,s}^{\text{Ada1}}}$ tends to 0 rapidly; (2) if ω tends to d_s , the product $\omega^{f_{i,s}^{\text{Ada0}}}(1 - \omega)^{f_{i,s}^{\text{Ada1}}}$ will be relatively far from 0. By the constraints of these requirements, we

design the following five types of $f_{i,s}^{\text{Ada0}}$ and $f_{i,s}^{\text{Ada1}}$, where the subscript $i = 1, 2, 3, 4, 5$ stands for Type1, Type2, Type3, Type4 and Type5, respectively.

Type 1:

$$f_{1,s}^{\text{Ada0}} = \frac{d_s}{m_s \omega + \epsilon_A}, f_{1,s}^{\text{Ada1}} = \frac{1 - d_s}{m_s(1 - \omega) + \epsilon_A}, \quad (10)$$

where $m_s \in \left[\frac{\alpha_s}{k+1}, M\right)$ with M being a finite positive constant real number. Here, α_s is a positive constant that depends on only the parameters r and s . A detailed description of α_s is given in Property 4 and its proof below, and the recommended values of α_s for different order WENO schemes are provided in Table 5 of Appendix A. In Eq.(10), ϵ_A is a very small positive number to prevent the denominator becoming zero, and the same holds for the following Eq.(12)(13). We will drop it in the theoretical analysis of this paper for simplicity.

Type 2:

$$f_{2,s}^{\text{Ada0}} = f_{2,s}^{\text{Ada1}} = \begin{cases} Q \cdot k, & \omega \leq \text{CFS}_s, \\ 1.0, & \text{CFS}_s < \omega < 1.0 - \frac{1.0 - d_s}{d_s} \times \text{CFS}_s, \\ Q \cdot k, & \omega \geq 1.0 - \frac{1.0 - d_s}{d_s} \times \text{CFS}_s, \end{cases} \quad (11)$$

where $Q \geq k^{-1}$, k is the same as in Eq.(16) and the Control Factor of Smoothness $\text{CFS}_s \in (0, d_s]$.

Type 3:

$$f_{3,s}^{\text{Ada0}} = f_{3,s}^{\text{Ada1}} = \frac{\max_{0 \leq j \leq 2} (\beta_j)}{\min_{0 \leq j \leq 2} (\beta_j) + \epsilon_A}. \quad (12)$$

Type 4:

$$f_{4,s}^{\text{Ada0}} = f_{4,s}^{\text{Ada1}} = \frac{\max_{0 \leq j \leq 2} \left(\frac{\omega_j}{d_j}\right)}{\min_{0 \leq j \leq 2} \left(\frac{\omega_j}{d_j}\right) + \epsilon_A}. \quad (13)$$

Type 5:

$$f_{5,s}^{\text{Ada0}} = f_{5,s}^{\text{Ada1}} = C, \quad (14)$$

where C is a constant and $C \geq 1$.

Remark 1. For simplicity, we mainly consider the case of Type 1 as an example in the following theoretical analysis. However, we present the mapping function curves and show the convergence order of the corresponding WENO schemes, as well as the numerical results, for the cases of Type 1 to Type 4. Here, we define Type 5 for completeness: it will be used only in the discussion of the mapping function curves as it is not truly adaptive.

3.2. A smoothing approximation to the signum function

To extend the range of the parameter k in the mapping functions of WENO-IM(k, A), we design a smoothing approximation to the well-known non-smoothing signum function as

$$sg(x, \delta) = \begin{cases} \frac{x}{|x|}, & |x| \geq \delta, \\ \frac{x}{(\delta^2 - x^2)^{k+3} + |x|}, & |x| < \delta. \end{cases} \quad (15)$$

where the constant $\delta > 0$ and $\delta \rightarrow 0$, $k \in \mathbb{N}^+$. It is trivial to verify the following properties.

Property 1. The smoothing approximation $sg(x, \delta)$ is $(k + 2)$ th-order differentiable.

Property 2. The smoothing approximation $sg(x, \delta)$ has the following properties:

- P1. $sg(x, \delta)$ is a bounded smoothing function;
- P2. if $x \neq 0$, then $sg(x, \delta) \neq 0$;
- P3. $sg(x, \delta)$ and x always have the same sign or we always have $sg(x, \delta) \cdot x^{2n-1} \geq 0, \forall n \in \mathbb{N}^+$;
- P4. $\frac{d}{dx}sg(x, \delta) \geq 0$;
- P5. $sg(0, \delta) = 0$ and $\frac{d}{dx}sg(0, \delta) \neq 0$;
- P6. if $|x| > \delta$, then $\frac{d}{dx}sg(x, \delta) = 0$.

As the proofs of the above two properties are simple, we do not provide them here.

3.3. A class of modified adaptive improved mapping functions

Now, employing the adaptive control functions $f_{i,s}^{Ada0}, f_{i,s}^{Ada1}$ and the smoothing approximation $sg(x, \delta)$, we propose a new family of modified adaptive mapping functions as

$$(g^{\text{MAIM}i})_s(\omega) = d_s + \frac{f_s^{\text{MAIM}} \cdot (\omega - d_s)^{k+1}}{f_s^{\text{MAIM}} \cdot (\omega - d_s)^k + \omega^{f_{i,s}^{Ada0}} (1 - \omega)^{f_{i,s}^{Ada1}}}, \quad k \in \mathbb{N}^+, A > 0, \quad (16)$$

where f_s^{MAIM} is a function of $\omega, A, k, d_s, \delta$ and it is defined as

$$f_s^{\text{MAIM}} = A \left(\frac{1 + (-1)^k}{2} + \frac{1 + (-1)^{k+1}}{2} \cdot sg(\omega - d_s, \delta) \right). \quad (17)$$

Notably, in our modified adaptive mapping functions, the parameter k is no longer limited to even integers but to all positive integers. Additionally, if one sets $k = 2n, n \in \mathbb{N}^+, A > 0$ and $f_{i,s}^{Ada0} = f_{i,s}^{Ada1} = 1$ (choosing $i = 5$ and $C = 1$), the family of mapping functions for WENO-IM(k, A) in [8] is obtained immediately. It means that the family of mapping functions of Feng et al. [8] belongs to our new family of modified adaptive mapping functions (16). Naturally, the mapping function proposed by Herick et al. in [16] also belongs to the new family of modified adaptive mapping functions by setting $k = 2, A = 1$ and $f_{i,s}^{Ada0} = f_{i,s}^{Ada1} = 1$.

Before giving Theorem 1 and its proof, we provide the following lemma and properties.

Lemma 4. The function f_s^{MAIM} satisfies:

- C1. it is a bounded smoothing function;
- C2. if $\omega \neq d_s$, then $f_s^{\text{MAIM}} \neq 0$;
- C3. $f_s^{\text{MAIM}} \cdot (\omega - d_s)^k \geq 0$;
- C4. $\frac{df_s^{\text{MAIM}}}{d\omega} \cdot (\omega - d_s)^{k+1} \geq 0$;
- C5. if $k = 2n, n \in \mathbb{N}^+$, then $f_s^{\text{MAIM}} \Big|_{\omega=d_s} \neq 0$, and if $k = 2n - 1, n \in \mathbb{N}^+$, then $f_s^{\text{MAIM}} \Big|_{\omega=d_s} = 0$ and $\frac{df_s^{\text{MAIM}}}{d\omega} \Big|_{\omega=d_s} \neq 0$;
- C6. f_s^{MAIM} is at least $(k + 2)$ th-order differentiable with respect to ω .

Proof.

(1) First, if $k = 2n, n \in \mathbb{N}^+$, we directly have $f_s^{\text{MAIM}} = A$. As A is a constant, $A > 0$, and $k = 2n, n \in \mathbb{N}^+$; thus, i) f_s^{MAIM} is bounded and smooth, then C1 is true; ii) for $\forall \omega \in [0, 1]$, we have $f_s^{\text{MAIM}} = A > 0$, then C2 is true; iii) C3 is true as $f_s^{\text{MAIM}} \cdot (\omega - d_s)^k = A \cdot (\omega - d_s)^{2n} \geq 0$; iv) C4 is true as $\frac{df_s^{\text{MAIM}}}{d\omega} \cdot (\omega - d_s)^{k+1} = \frac{dA}{d\omega} \cdot (\omega - d_s)^{k+1} = 0$; v) for $\forall \omega \in [0, 1]$, we have $f_s^{\text{MAIM}} = A \neq 0$, then C5 is true; vi) C6 is true as $\frac{d^q f_s^{\text{MAIM}}}{d\omega^q} = \frac{d^q A}{d\omega^q} = 0, \forall q \in \mathbb{N}^+$.

(2) Then, we give the proof in the case that $k = 2n - 1, n \in \mathbb{N}^+$. At present, we can rewrite Eq.(17) as

$$f_s^{\text{MAIM}} = A \cdot sg(\omega - d_s, \delta).$$

As A is a constant, $A > 0$, and $k = 2n - 1, n \in \mathbb{N}^+$, letting $x = \omega - d_s$ and substituting it into Eq.(15), we obtain the following results trivially: i) according to P1 of Property 2, we know that f_s^{MAIM} is bounded and smooth, then C1 is true; ii) if $\omega \neq d_s \Rightarrow x \neq 0 \Rightarrow$ P2 of Property 2 is satisfied, then $f_s^{\text{MAIM}} \neq 0$ and C2 is true; iii) if $k = 2n - 1, n \in \mathbb{N}^+ \Rightarrow$

$P3$ of Property 2 is satisfied, then $f_s^{\text{MAIM}} \cdot (\omega - d_s)^k \geq 0$ and $C3$ is true; iv) according to $P4$ of Property 2, we have $\frac{df_s^{\text{MAIM}}}{d\omega} = sg(x, \delta) \frac{dA}{dx} + A \frac{dsg(x, \delta)}{dx} \geq 0$, and it is easy to find that $(\omega - d_s)^{k+1} \geq 0$, ($k = 2n - 1, n \in \mathbb{N}^+$), thus $\frac{df_s^{\text{MAIM}}}{d\omega} \cdot (\omega - d_s)^{k+1} \geq 0$ and $C4$ is true; v) as $\omega = d_s$, namely, $x = 0$, so $P5$ of Property 2 is satisfied, then we have $f_s^{\text{MAIM}} \Big|_{\omega=d_s} = A \cdot sg(\omega - d_s, \delta) \Big|_{\omega=d_s} = 0$ and $\frac{df_s^{\text{MAIM}}}{d\omega} \Big|_{\omega=d_s} = \left(A \frac{d}{dx} sg(x, \delta) + sg(x, \delta) \frac{dA}{dx} \right) \Big|_{x=0} \neq 0$, thus, $C5$ is true; vi) as A is a constant, we obtain $\frac{d^m A}{dx^m} = 0, \forall m \in \mathbb{N}^+$, and according to Property 1, we have $sg(x, \delta) \in C^{k+2}(\mathbb{R})$, thus, $C6$ is true as $\frac{d^q f_s^{\text{MAIM}}}{d\omega^q} = A \frac{d^q}{dx^q} sg(x, \delta), q = 1, 2, \dots, k + 2$. \square

Property 3. *Let*

$$q_s(\omega) = (\omega - d_s) \left(\frac{d_s}{\omega^2} (1 - \ln \omega) + \frac{1 - d_s}{(1 - \omega)^2} (\ln(1 - \omega) - 1) \right), \quad \omega \in (0, 1)$$

then, the maximum value of $q_s(\omega)$ is finite for all optimal weights d_s in various $(2r - 1)$ th-order WENO schemes with $r \in \{2, \dots, 9\}$ (the values of all these d_s can be found in Table 3 of [9]).

Proof.

After simple mathematical manipulations, we obtain

$$q'_s(\omega) = \frac{d_s}{\omega^2} (1 - \ln \omega) + \frac{1 - d_s}{(1 - \omega)^2} (\ln(1 - \omega) - 1) + (\omega - d_s) \left(-\frac{2d_s}{\omega^3} (1 - \ln \omega) - \frac{d_s}{\omega^3} + \frac{2(1 - d_s)}{(1 - \omega)^3} (\ln(1 - \omega) - 1) - \frac{1 - d_s}{(1 - \omega)^3} \right).$$

Clearly, $q'_s(\omega)$ is continuous in $(0, 1)$. Therefore, if we can verify that there is one and only one value of $\omega \in (0, 1)$, namely, ω_{crit} , satisfying $q'_s(\omega_{\text{crit}}) = 0, q'_s(\omega) > 0, \forall \omega \in (0, \omega_{\text{crit}})$ and $q'_s(\omega) < 0, \forall \omega \in (\omega_{\text{crit}}, 1)$, we can prove Property 3. Unfortunately, this direct theoretical verification is challenging. However, for a fixed value of d_s , we can easily obtain the solution of $q'_s(\omega) = 0$ and get the curve of $q'_s(\omega)$ by numerical means. After extensive calculations using software MATLAB, we found that, for every optimal weight d_s in various $(2r - 1)$ th-order WENO schemes with $r \in \{2, \dots, 9\}$, the requirements of $q'_s(\omega) = 0, q'_s(\omega) > 0$ for $\omega \in (0, \omega_{\text{crit}})$ and $q'_s(\omega) < 0$ for $\omega \in (\omega_{\text{crit}}, 1)$ are all satisfied. We show the maximum value of $q_s(\omega)$ for various $(2r - 1)$ th-order WENO schemes with $r \in \{2, \dots, 9\}$ in Table 5 in Appendix A. \square

Property 4. *Let $T_s(\omega) = \omega \frac{d_s}{m_s \omega} \cdot (1 - \omega)^{\frac{1 - d_s}{m_s}}$, $Q_s(\omega) = k + 1 - \frac{q_s(\omega)}{m_s}$ and $P_s(\omega) = T_s(\omega) Q_s(\omega)$, then, $T_s(\omega), Q_s(\omega), P_s(\omega)$ possess the following properties:*

P1. $T_s(\omega) \geq 0, \forall \omega \in [0, 1]$ and $\lim_{\omega \rightarrow 0^+} T_s(\omega) = \lim_{\omega \rightarrow 1^-} T_s(\omega) = 0$;

P2. if $m_s \in \left[\frac{\alpha_s}{k+1}, M \right)$, where M is a finite positive constant real number and $\alpha_s > \max_{0 < \omega < 1} (0, \max_{0 < \omega < 1} q_s(\omega))$, then $Q_s(\omega) > 0, \forall \omega \in (0, 1)$;

P3. $\lim_{\omega \rightarrow 0^+} P_s(\omega) = \lim_{\omega \rightarrow 1^-} P_s(\omega) = 0$.

Proof.

(1) It is easy to verify $P1$ of Property 4, as $\omega \in [0, 1]$ and $\frac{d_s}{m_s \omega} > 0, \frac{1 - d_s}{m_s(1 - \omega)} > 0$.

(2) Clearly, when $q_s(\omega) \leq 0$, we have $Q_s(\omega) > 0$ as $m_s > 0$. If $q_s(\omega) > 0$, as $m_s \in \left[\frac{\alpha_s}{k+1}, M \right)$, according to Property 3, we have

$$Q_s(\omega) = k + 1 - \frac{q_s(\omega)}{m_s} \geq k + 1 - \frac{k + 1}{\alpha_s} q_s(\omega) > (k + 1) \left(1 - \frac{q_s(\omega)}{\max_{0 < \omega < 1} q_s(\omega)} \right) \geq (k + 1) \left(1 - \frac{\max_{0 < \omega < 1} q_s(\omega)}{\max_{0 < \omega < 1} q_s(\omega)} \right) = 0.$$

Thus, $P2$ of Property 4 is true.

(3) If $n > 0$, by employing L'Hospital's Rule, it is trivial to show that

$$\lim_{x \rightarrow 0^+} \left(x^n \ln \frac{1}{x} \right) = \lim_{x \rightarrow 0^+} \frac{\ln \frac{1}{x}}{\left(\frac{1}{x} \right)^n} = \lim_{t \rightarrow +\infty} \frac{\ln t}{t^n} = \lim_{t \rightarrow +\infty} \frac{1}{nt^n} = 0.$$

Then, as $\lim_{\omega \rightarrow 0^+} \left(\frac{d_s}{m_s \omega} - 2 \right) \gg 0$ and $\lim_{\omega \rightarrow 1^-} \left(\frac{1-d_s}{m_s(1-\omega)} - 2 \right) = \lim_{\tilde{\omega} \rightarrow 0^+} \left(\frac{1-d_s}{m_s \tilde{\omega}} - 2 \right) \gg 0$, we obtain

$$\begin{aligned} \lim_{\omega \rightarrow 0^+} \left(\omega^{\frac{d_s}{m_s \omega}} \frac{1}{\omega^2} (-\ln \omega) \right) &= \lim_{\omega \rightarrow 0^+} \left(\omega^{\frac{d_s}{m_s \omega} - 2} \ln \frac{1}{\omega} \right) = 0, \\ \lim_{\omega \rightarrow 1^-} \left((1-\omega)^{\frac{1-d_s}{m_s(1-\omega)}} \frac{1}{(1-\omega)^2} \ln(1-\omega) \right) &= \lim_{\tilde{\omega} \rightarrow 0^+} \left(-\tilde{\omega}^{\frac{1-d_s}{m_s \tilde{\omega}} - 2} \ln \frac{1}{\tilde{\omega}} \right) = 0. \end{aligned}$$

Now, we can prove P3 of Property 4 as

$$\begin{aligned} \lim_{\omega \rightarrow 0^+} P_s(\omega) &= \lim_{\omega \rightarrow 0^+} \left\{ \omega^{\frac{d_s}{m_s \omega}} \cdot (1-\omega)^{\frac{1-d_s}{m_s(1-\omega)}} \left(k+1 - \frac{1}{m_s}(\omega-d_s) \left(\frac{d_s}{\omega^2} (1-\ln \omega) + \frac{1-d_s}{(1-\omega)^2} (\ln(1-\omega) - 1) \right) \right) \right\} \\ &= \lim_{\omega \rightarrow 0^+} \left\{ (k+1) \cdot (1-\omega)^{\frac{1-d_s}{m_s(1-\omega)}} \times \left(\omega^{\frac{d_s}{m_s \omega}} \right) \right\} \\ &+ \lim_{\omega \rightarrow 0^+} \left\{ -\frac{d_s}{m_s} (\omega-d_s) \cdot (1-\omega)^{\frac{1-d_s}{m_s(1-\omega)}} \times \left(\omega^{\frac{d_s}{m_s \omega} - 2} \right) \right\} \\ &+ \lim_{\omega \rightarrow 0^+} \left\{ -\frac{d_s}{m_s} (\omega-d_s) \cdot (1-\omega)^{\frac{1-d_s}{m_s(1-\omega)}} \times \left(\omega^{\frac{d_s}{m_s \omega}} \frac{1}{\omega^2} (-\ln \omega) \right) \right\} \\ &+ \lim_{\omega \rightarrow 0^+} \left\{ -\frac{1-d_s}{m_s} (\omega-d_s) \cdot (1-\omega)^{\frac{1-d_s}{m_s(1-\omega)}} \cdot \frac{\ln(1-\omega) - 1}{(1-\omega)^2} \times \left(\omega^{\frac{d_s}{m_s \omega}} \right) \right\} \\ &= 0, \end{aligned}$$

and

$$\begin{aligned} \lim_{\omega \rightarrow 1^-} P_s(\omega) &= \lim_{\omega \rightarrow 1^-} \left\{ \omega^{\frac{d_s}{m_s \omega}} \cdot (1-\omega)^{\frac{1-d_s}{m_s(1-\omega)}} \left(k+1 - \frac{1}{m_s}(\omega-d_s) \left(\frac{d_s}{\omega^2} (1-\ln \omega) + \frac{1-d_s}{(1-\omega)^2} (\ln(1-\omega) - 1) \right) \right) \right\} \\ &= \lim_{\omega \rightarrow 1^-} \left\{ (k+1) \cdot \omega^{\frac{d_s}{m_s \omega}} \times \left((1-\omega)^{\frac{1-d_s}{m_s(1-\omega)}} \right) \right\} \\ &+ \lim_{\omega \rightarrow 1^-} \left\{ -\frac{d_s}{m_s} (\omega-d_s) \cdot \omega^{\frac{d_s}{m_s \omega}} \cdot \frac{1-\ln \omega}{\omega^2} \times \left((1-\omega)^{\frac{1-d_s}{m_s(1-\omega)}} \right) \right\} \\ &+ \lim_{\omega \rightarrow 1^-} \left\{ -\frac{1-d_s}{m_s} (\omega-d_s) \cdot \omega^{\frac{d_s}{m_s \omega}} \times \left((1-\omega)^{\frac{1-d_s}{m_s(1-\omega)}} \frac{1}{(1-\omega)^2} \ln(1-\omega) \right) \right\} \\ &+ \lim_{\omega \rightarrow 1^-} \left\{ -\frac{1-d_s}{m_s} (\omega-d_s) \cdot \omega^{\frac{d_s}{m_s \omega}} \times \left(- (1-\omega)^{\frac{1-d_s}{m_s(1-\omega)} - 2} \right) \right\} \\ &= 0. \end{aligned}$$

□

Theorem 1. *If the mapping functions are defined by Eq.(10) and Eq.(16), they satisfy:*

- C1. $(g^{\text{MAIM1}})_s(0) = 0, (g^{\text{MAIM1}})_s(1) = 1, (g^{\text{MAIM1}})_s(d_s) = d_s$;
- C2. $(g^{\text{MAIM1}})'_s(\omega) \geq 0$, if $\omega \in (0, 1)$;
- C3. *If $k = 2n, n \in \mathbb{N}^+$, then $(g^{\text{MAIM1}})'_s(d_s) = (g^{\text{MAIM1}})''_s(d_s) = \dots = (g^{\text{MAIM1}})^{(k)}_s(d_s) = 0, (g^{\text{MAIM1}})^{(k+1)}_s(d_s) \neq 0$, and if $k = 2n - 1, n \in \mathbb{N}^+$, then $(g^{\text{MAIM1}})'_s(d_s) = (g^{\text{MAIM1}})''_s(d_s) = \dots = (g^{\text{MAIM1}})^{(k+1)}_s(d_s) = 0, (g^{\text{MAIM1}})^{(k+2)}_s(d_s) \neq 0$;*
- C4. $(g^{\text{MAIM1}})'_s(0^+) = (g^{\text{MAIM1}})'_s(1^-) = 1$ for $m_s \in \left[\frac{\alpha_s}{k+1}, M \right)$, where M is a finite positive constant real number and $\alpha_s > \max(0, \max_{0 < \omega < 1} q_s(\omega))$.

Proof.

As the bounded smoothing functions f_s^{MAIM} satisfy conditions C2 and C3 of Lemma 4 and $d_s \in (0, 1)$, we have

$$f_s^{\text{MAIM}} \cdot (\omega - d_s)^k + \omega^{f_{1,s}^{\text{Ada0}}} (1-\omega)^{f_{1,s}^{\text{Ada1}}} > 0, \quad \forall \omega \in [0, 1].$$

Therefore, the denominator of Eq.(16) will never be zero; in other words, Eq.(16) will always make sense. Thus, one can design the mapping functions according to Eq.(10) and Eq.(16). Next, we prove $C1 \sim C4$ of Theorem 1.

(1) According to the $C2$ of Lemma 4 and $d_s \in (0, 1)$, we can obtain $f_s^{\text{MAIM}}|_{\omega=0} \neq 0$ and $f_s^{\text{MAIM}}|_{\omega=1} \neq 0$; then,

$$\begin{aligned} (g^{\text{MAIM1}})_s(\omega)|_{\omega=0} &= d_s + \frac{f_s^{\text{MAIM}} \cdot (\omega - d_s)^{k+1}}{f_s^{\text{MAIM}} \cdot (\omega - d_s)^k} \Big|_{\omega=0} = d_s - d_s = 0, \\ (g^{\text{MAIM1}})_s(\omega)|_{\omega=1} &= d_s + \frac{f_s^{\text{MAIM}} \cdot (\omega - d_s)^{k+1}}{f_s^{\text{MAIM}} \cdot (\omega - d_s)^k} \Big|_{\omega=1} = d_s + (1 - d_s) = 1. \end{aligned}$$

From the $C1$ of Lemma 4, we know $f_s^{\text{MAIM}} \cdot (\omega - d_s)^{k+1}|_{\omega=d_s} = 0$, so

$$(g^{\text{MAIM1}})_s(\omega)|_{\omega=d_s} = d_s + \frac{0}{d_s(1-d_s)} = d_s.$$

(2) As the parameter ϵ_A in Eq.(10) is a very small number used only to prevent the denominator becoming zero, we drop it in the theoretical analysis. Then, taking the derivative of $(g^{\text{MAIM1}})_s(\omega)$ with respect to ω , we obtain

$$(g^{\text{MAIM1}})'_s(\omega) = \frac{P_{\text{num}}(\omega)}{P_{\text{den}}(\omega)} = \frac{(f_s^{\text{MAIM}})^2 \cdot (\omega - d_s)^{2k} + \frac{df_s^{\text{MAIM}}}{d\omega} \cdot (\omega - d_s)^{k+1} T_s(\omega) + f_s^{\text{MAIM}} \cdot (\omega - d_s)^k P_s(\omega)}{\left(f_s^{\text{MAIM}} \cdot (\omega - d_s)^k + T_s(\omega)\right)^2}, \quad (18)$$

where $P_s(\omega), T_s(\omega), Q_s(\omega)$ are the same as in Property 4.

For $m_s \in \left[\frac{\epsilon_A}{k+1}, M\right)$, according to $P1$ and $P2$ of Property 4, we have $T_s(\omega) \geq 0, Q_s(\omega) > 0, \forall \omega \in (0, 1)$. By employing the conditions $C3$ and $C4$ of Lemma 4 and considering $(f_s^{\text{MAIM}})^2 \geq 0, (\omega - d_s)^{2k} \geq 0$, we conclude that

$$(g^{\text{MAIM1}})'_s(\omega) \geq 0, \quad \forall \omega \in (0, 1).$$

(3) As $f_s^{\text{MAIM}} \in C^{k+2}(\mathbb{R})$, which has been provided by $C6$ of Lemma 4, $(g^{\text{MAIM1}})_s^{(q)}(\omega)$ always makes sense for $q = 1, 2, \dots, k+2$.

i) If $k = 2n, n \in \mathbb{N}^+$, we know that $f_s^{\text{MAIM}} \neq 0$; then, $(\omega - d_s)^k \mid P_{\text{num}}$, and $(\omega - d_s)^{k+1} \nmid P_{\text{num}}$. As $T_s(\omega)Q_s(\omega) > 0, \forall \omega \in (0, 1)$, we obtain

$$(g^{\text{MAIM1}})'_s(d_s) = (g^{\text{MAIM1}})''_s(d_s) = \dots = (g^{\text{MAIM1}})_s^{(k)}(d_s) = 0, (g^{\text{MAIM1}})_s^{(k+1)}(d_s) \neq 0.$$

ii) If $k = 2n - 1, n \in \mathbb{N}^+$, we have $f_s^{\text{MAIM}} = 0$ and $\frac{df_s^{\text{MAIM}}}{d\omega} \neq 0$; then, $(\omega - d_s)^{k+1} \mid P_{\text{num}}$, and $(\omega - d_s)^{k+2} \nmid P_{\text{num}}$. Similarly, as $T_s(\omega)Q_s(\omega) > 0, \forall \omega \in (0, 1)$, we obtain

$$(g^{\text{MAIM1}})'_s(d_s) = (g^{\text{MAIM1}})''_s(d_s) = \dots = (g^{\text{MAIM1}})_s^{(k+1)}(d_s) = 0, (g^{\text{MAIM1}})_s^{(k+2)}(d_s) \neq 0.$$

(4) According to $P1$ and $P3$ of Property 4 and the fact of $P6$ of Property 2, from Eq.(18), it is very easy to obtain

$$\begin{aligned} (g^{\text{MAIM1}})'_s(0^+) &= \frac{(f_s^{\text{MAIM}})^2 \cdot (\omega - d_s)^{2k} + \frac{df_s^{\text{MAIM}}}{d\omega} \cdot (\omega - d_s)^{k+1} \lim_{\omega \rightarrow 0^+} T_s(\omega) + f_s^{\text{MAIM}} \cdot (\omega - d_s)^k \lim_{\omega \rightarrow 0^+} P_s(\omega)}{(f_s^{\text{MAIM}} \cdot (\omega - d_s)^k + \lim_{\omega \rightarrow 0^+} T_s(\omega))^2} \\ &= \frac{(f_s^{\text{MAIM}})^2 \cdot (\omega - d_s)^{2k}}{(f_s^{\text{MAIM}} \cdot (\omega - d_s)^k)^2} = 1. \end{aligned}$$

and

$$\begin{aligned} (g^{\text{MAIM1}})'_s(1^-) &= \frac{(f_s^{\text{MAIM}})^2 \cdot (\omega - d_s)^{2k} + \frac{df_s^{\text{MAIM}}}{d\omega} \cdot (\omega - d_s)^{k+1} \lim_{\omega \rightarrow 1^-} T_s(\omega) + f_s^{\text{MAIM}} \cdot (\omega - d_s)^k \lim_{\omega \rightarrow 1^-} P_s(\omega)}{(f_s^{\text{MAIM}} \cdot (\omega - d_s)^k + \lim_{\omega \rightarrow 1^-} T_s(\omega))^2} \\ &= \frac{(f_s^{\text{MAIM}})^2 \cdot (\omega - d_s)^{2k}}{(f_s^{\text{MAIM}} \cdot (\omega - d_s)^k)^2} = 1. \end{aligned}$$

□

Corollary 1. *If the adaptive mapping function is defined by Eq.(16), with the functions $f_{i,s}^{\text{Ada0}}, f_{i,s}^{\text{Ada1}}$ calculated by Eq.(11) or Eq.(14), the mapping function has the properties proposed in Theorem 1.*

Corollary 2. *In smooth regions, if the adaptive mapping function is defined by Eq.(16), with the functions $f_{i,s}^{\text{Ada0}}, f_{i,s}^{\text{Ada1}}$ calculated by Eq.(12) or Eq.(13), the mapping function has the properties proposed in Theorem 1.*

Remark 2. *The proof of Corollary 1 is very similar to that of Theorem 1, especially for $(g^{\text{MAIM5}})_s(\omega)$ with $f_{5,s}^{\text{Ada0}}, f_{5,s}^{\text{Ada1}}$ defined by Eq.(14). For Corollary 2, when in smooth regions, we can treat $f_{3,s}^{\text{Ada0}}, f_{3,s}^{\text{Ada1}}$ in Eq.(12) and $f_{4,s}^{\text{Ada0}}, f_{4,s}^{\text{Ada1}}$ in Eq.(13) as constants; then, the proof is almost the same as that of $(g^{\text{MAIM5}})_s(\omega)$ with $f_{5,s}^{\text{Ada0}}, f_{5,s}^{\text{Ada1}}$ defined by Eq.(14).*

Remark 3. *Notably, for problems with discontinuities, if the adaptive mapping function is defined by Eq.(16), with the functions $f_{i,s}^{\text{Ada0}}, f_{i,s}^{\text{Ada1}}$ calculated by Eq.(12) or Eq.(13), the mapping function will only have property C1 proposed in Theorem 1, and properties C2, C3, C4 are not satisfied. We verify these conclusions in subsection 3.4.2.*

3.4. The new WENO schemes

Now, we give the new mapped weights as follows

$$\omega_s^{\text{MAIM}i} = \frac{\alpha_s^{\text{MAIM}i}}{\sum_{l=0}^2 \alpha_l^{\text{MAIM}i}}, \alpha_s^{\text{MAIM}i} = (g^{\text{MAIM}i})_s(\omega_s^{\text{JS}}).$$

We denote the new family of modified adaptive improved mapped schemes using the weights $\omega_s^{\text{MAIM}i}$ as WENO-MAIM1($k = \cdot, A = \cdot, m_s = \cdot$), WENO-MAIM2($k = \cdot, A = \cdot, Q = \cdot, \text{CFS}_s = \cdot$), WENO-MAIM3($k = \cdot, A = \cdot$), WENO-MAIM4($k = \cdot, A = \cdot$) and WENO-MAIM5($k = \cdot, A = \cdot, C = \cdot$), respectively. For simplicity, we use WENO-MAIM i without confusion.

3.4.1. The role of f_s^{MAIM}

We now explain that for the case of $k = 2n - 1, n \in \mathbb{N}^+$, the quotient of f_s^{MAIM} and A from Eq.(17) is only an approximation of the signum function but does not tend to $\omega - d_s$. In other words, when $k = 2n - 1, n \in \mathbb{N}^+$, the product $f_s^{\text{MAIM}} \cdot (\omega - d_s)^k$ in Eq.(16) is entirely different from $A(\omega - d_s)^{k+1}$. To illustrate this result, we take the following linear advection equation with the periodic boundary conditions as an example

$$\begin{cases} u_t + u_x = 0, & -1 \leq x \leq 1, \\ u(x, 0) = \sin(\pi x), \end{cases} \quad (19)$$

where the output time is $t = 2.0$ and the number of cells is $N = 800$. Without loss of generality, we employ the fifth-order WENO-MAIM1 scheme and set $\delta = 10^{-6}$ (the same holds in the rest of this paper), $k = 1, A = 10^{-6}$ for f_s^{MAIM} and $m_s = 0.5, \epsilon_A = 10^{-100}$ for $f_{1,s}^{\text{Ada0}}, f_{1,s}^{\text{Ada1}}$. The comparison of $\frac{f_s^{\text{MAIM}}}{A}$ and $\omega - d_s$, taking $d_1 = 0.6$ as an example, is shown in Fig.1. From Fig.1, we intuitively find that $\frac{f_s^{\text{MAIM}}}{A}$ is only an approximation of the signum function but does not tend to $\omega - d_s$. The same results have been achieved for $d_0 = 0.3$ and $d_2 = 0.1$.

3.4.2. Parametric study of the mapping functions

We can consider the WENO-JS scheme as a mapped WENO scheme with a mapping function defined as $(g^{\text{JS}})_s(\omega) = \omega$. Then, it can be easily verified that $(g^{\text{MAIM1}})_s(\omega)|_{m_s \rightarrow 0} = (g^{\text{JS}})_s(\omega), (g^{\text{MAIM5}})_s(\omega)|_{k=2, A=1, C=1} = (g^{\text{M}})_s(\omega), (g^{\text{MAIM5}})_s(\omega)|_{k=2, A=0.1, C=1} = (g^{\text{IM}})_s(\omega; 2, 0.1)$. We present these results directly in Fig.2(a). For $(g^{\text{MAIM1}})_s(\omega)$, we have the following properties: (1) for given k and A , decreasing m_s will make the function follow the identity map more closely but to narrow the optimal weight interval (see Fig.2(b)), and the optimal weight interval stands for the interval about $\omega = d_s$ over which the mapping process attempts to use the corresponding optimal weight; (2) for given A and m_s , the optimal weight interval is widened by increasing k as more derivatives vanish at $\omega = d_s$ (see Fig.2(c)); (3) for given k and m_s , the optimal weight interval is narrowed by increasing A (see Fig.2(d)).

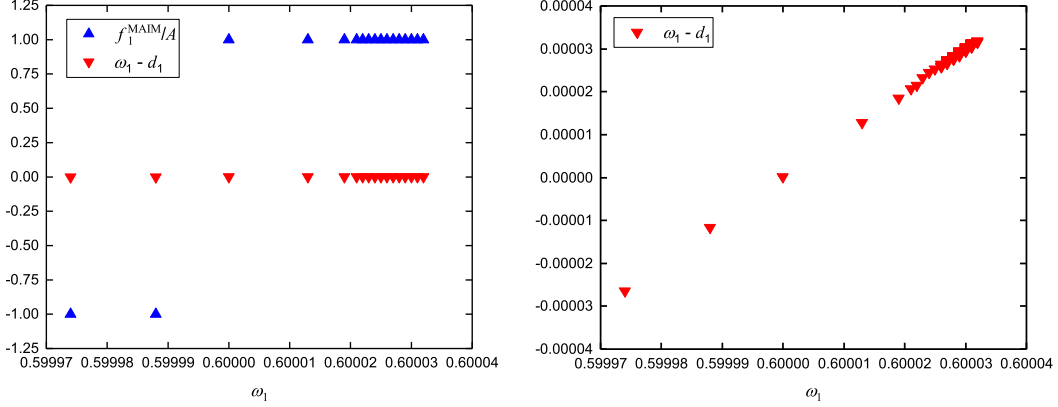


Fig. 1. Comparison of $\frac{f_1^{\text{MAIM}}}{A}$ and $\omega - d_1$ for $d_1 = 0.6$ (left: full; right: zoomed).

For $(g^{\text{MAIM2}})_s(\omega)$, it is trivial to show that $(g^{\text{MAIM2}})_s(\omega)|_{k=1, A=0.01, Q=100, \text{CFS}_s=1} = (g^{\text{JS}})_s(\omega)$, $(g^{\text{MAIM2}})_s(\omega)|_{k=2, A=1, \text{CFS}_s=0} = (g^{\text{M}})_s(\omega)$, $(g^{\text{MAIM2}})_s(\omega)|_{k=2, A=0.1, \text{CFS}_s=0} = (g^{\text{IM}})_s(\omega; 2, 0.1)$. We illustrate these results directly in Fig.3(a). Similarly, for $(g^{\text{MAIM2}})_s(\omega)$, we have the following properties: (1) for given k, A and CFS_s , increasing Q makes the function follow the identity map more closely and narrow the optimal weight interval down to the minimum optimal weight interval controlled by the parameter CFS_s (see Fig.3(b)); (2) for given k, A and Q , the optimal weight interval is widened by decreasing CFS_s (see Fig.3(c)); (3) the effects of parameters k and A are the same as in $(g^{\text{MAIM1}})_s(\omega)$, but one must consider the effect of the parameter CFS_s (see Fig.3(d)).

The study of the mapping functions $(g^{\text{MAIM3}})_s(\omega)$ and $(g^{\text{MAIM4}})_s(\omega)$ is slightly more complicated as these functions are not independent functions of ω : one must obtain the relationship of $(g^{\text{MAIM3}})_s(\omega) \sim \omega$ or $(g^{\text{MAIM4}})_s(\omega) \sim \omega$ by specific numerical examples. We found that if the problem is non-smooth, these mapping functions will not maintain the monotonicity property. To illustrate this result, we take the linear advection equation $u_t + u_x = 0$ as an example with the following initial condition consisting of two constant states separated by sharp discontinuities at $x = 0, \pm 1$

$$u(x, 0) = \begin{cases} 1, & x \in [-1, 0), \\ 0, & x \in [0, 1]. \end{cases} \quad (20)$$

The results are shown in Fig.4 at the resolution $N = 200$ cells and output time $t = 200$. In the calculations, the CFL number is chosen to be 0.1 and the periodic boundary conditions in two directions are used. From Fig.4, we see that the mapping functions $(g^{\text{MAIM3}})_s(\omega)$ and $(g^{\text{MAIM4}})_s(\omega)$ are non-monotonic with respect to ω for non-smooth problems. However, the monotonicity of the mapping functions $(g^{\text{MAIM1}})_s(\omega)$ and $(g^{\text{MAIM2}})_s(\omega)$ with respect to ω can be maintained very well.

3.4.3. The rate of convergence

WENO schemes up to 17th-order of accuracy have been outlined by Gerolymos et al. in [9]. Notationally, let $n_{\text{cp}} \in \mathbb{N}$ denote the order of the critical point; that is, if $n_{\text{cp}} = k_{\text{crit}}$, then $f' = \dots = f^{(k_{\text{crit}})} = 0$ and $f^{(k_{\text{crit}}+1)} \neq 0$. Now, we present Theorem 2, which will show that the WENO-MAIM i schemes can recover the optimal convergence rates by setting the parameter k for different values of n_{cp} in smooth regions.

Theorem 2. Let $\lceil x \rceil$ be a ceiling function of x , for $n_{\text{cp}} < r - 1$, the WENO-MAIM i schemes can achieve the optimal $(2r - 1)$ th-order of accuracy if the modified adaptive improved mapping functions $(g^{\text{MAIM}i})_s(\omega)$ defined in Eq.(16) are applied to the original weights in the WENO-JS scheme with $k \geq k^{\text{MAIM}}$, where

$$k^{\text{MAIM}} = \left\lceil \frac{r}{r-1-n_{\text{cp}}} - 2 \right\rceil + \frac{1 + \left(-1 \right)^{\left\lceil \frac{r}{r-1-n_{\text{cp}}} - 2 \right\rceil}}{2}. \quad (21)$$

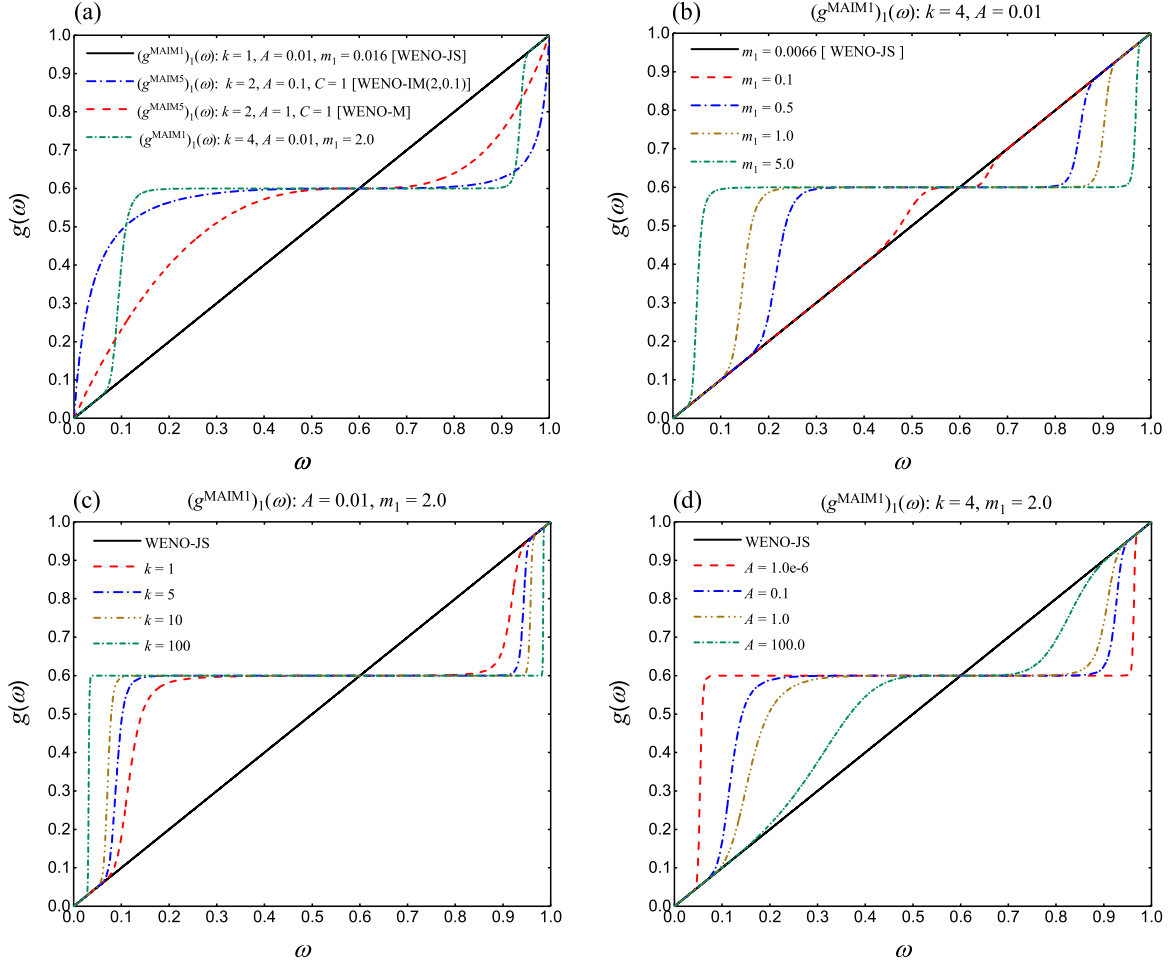


Fig. 2. New mapping functions $(g^{\text{MAIM1}})_1(\omega)$, $(g^{\text{MAIMS}})_1(\omega)$, and effect of varying parameters k, A and m_s on $(g^{\text{MAIM1}})_1(\omega)$ for $d_1 = 0.6$.

Before giving the proof of Theorem 2, we state the following two lemmas.

Lemma 5. When $n_{\text{cp}} < r - 1$, the weights ω_s^{JS} in the $(2r - 1)$ th-order WENO-JS scheme satisfy

$$\omega_s^{\text{JS}} - d_s = O(\Delta x^{r-1-n_{\text{cp}}}), \quad r = 2, 3, \dots, 9, \quad (22)$$

then, the convergence order is

$$r_c = \begin{cases} 2r - 1, & \text{if } n_{\text{cp}} = 0, \\ 2r - 2 - n_{\text{cp}}, & \text{if } n_{\text{cp}} = 1, 2, \dots, r - 1. \end{cases}$$

The above lemma is a direct extension of Lemma 2 in [8], and we only extend the range of r from $r = 2, 3, \dots, 6$ to $r = 2, 3, \dots, 9$. As the proof of the lemma can be found on page 565 in [16], we simply state it explicitly here.

Lemma 6. For $r = 2, 3, \dots, 9$, the sufficient condition for the $(2r - 1)$ th-order WENO scheme to achieve the optimal order of accuracy is

$$\omega_s - d_s = O(\Delta x^r), \quad s = 0, 1, \dots, r - 1.$$

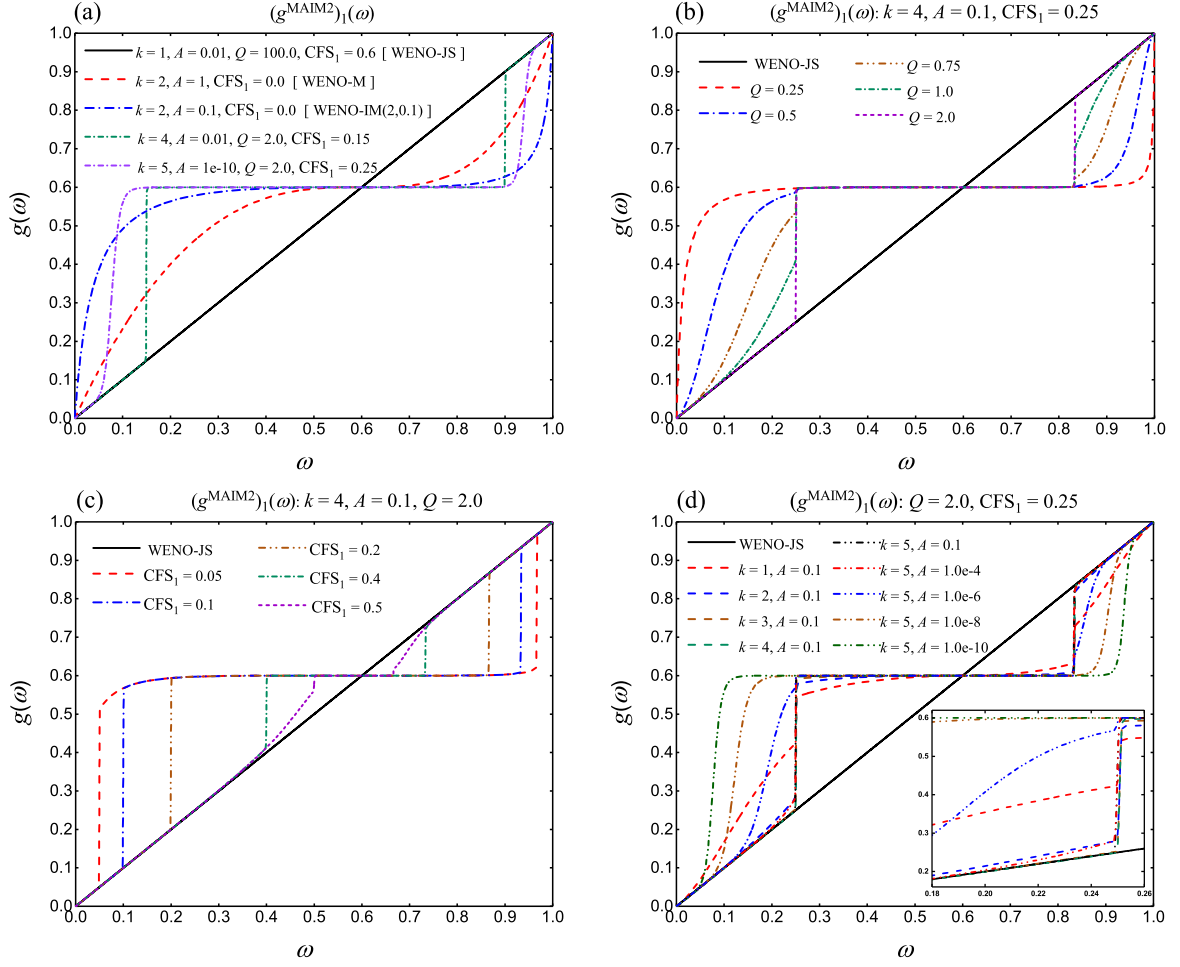


Fig. 3. Effect of varying parameters k , A , Q and CFS_s on $(g^{\text{MAIM2}})_1(\omega)$ for $d_1 = 0.6$.

Remark 4. The proof of Lemma 6 in this paper is the finite volume version of Lemma 1 in [8], which is a natural extension of the one in [16]. For more details about the proof within the finite volume framework, the reference [31] is referred to.

Proof of Theorem 2.

(1) If $k = 2n$, $n \in \mathbb{N}^+$, from Theorem 1, Corollary 1 and Corollary 2, we have $(g^{\text{MAIMi}})_s(d_s) = d_s$ and $(g^{\text{MAIMi}})'_s(d_s) = (g^{\text{MAIMi}})''_s(d_s) = \dots = (g^{\text{MAIMi}})^{(k)}_s(d_s) = 0$, $(g^{\text{MAIMi}})^{(k+1)}_s(d_s) \neq 0$. Thus, evaluation at ω_s^{JS} of the Taylor series approximation of the $(g^{\text{MAIMi}})_s(\omega)$ about d_s yields

$$\begin{aligned} \alpha_s^{\text{MAIMi}} &= (g^{\text{MAIMi}})_s(d_s) + \sum_{l=1}^k \frac{(g^{\text{MAIMi}})^{(l)}_s(d_s)}{l!} (\omega_s^{\text{JS}} - d_s)^l + \frac{(g^{\text{MAIMi}})^{(k+1)}_s(d_s)}{(k+1)!} (\omega_s^{\text{JS}} - d_s)^{k+1} + \dots \\ &= d_s + \frac{(g^{\text{MAIMi}})^{(k+1)}_s(d_s)}{(k+1)!} (\omega_s^{\text{JS}} - d_s)^{k+1} + \dots \end{aligned}$$

According to Lemma 5 and Lemma 6, the $(2r-1)$ th-order WENO-MAIMi schemes can achieve the optimal $(2r-1)$ th-order of accuracy with requirement

$$(r-1-n_{\text{cp}})(k+1) \geq r, \quad 1 \leq n_{\text{cp}} < r-1.$$

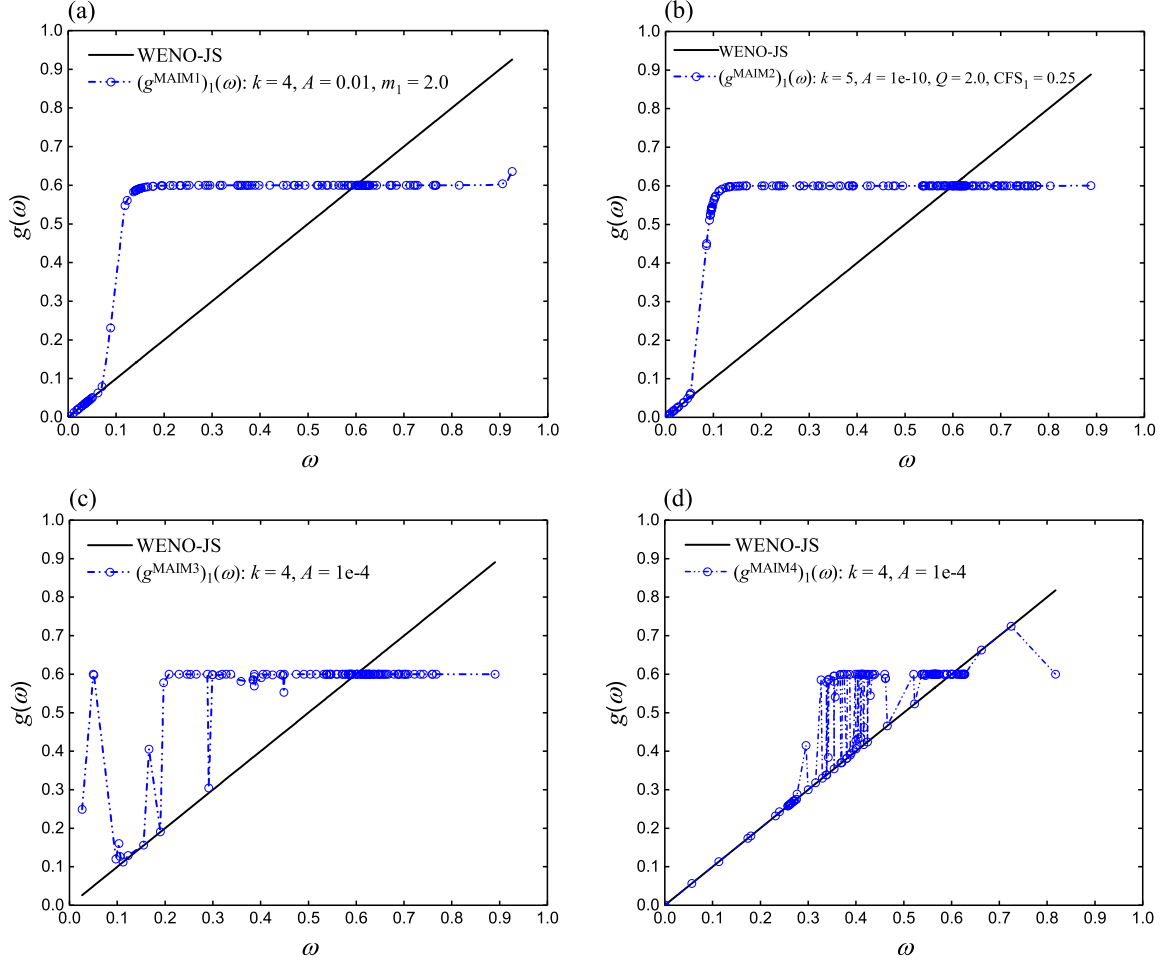


Fig. 4. Comparison of the mapping functions $(g^{\text{MAIM1}})_1(\omega)$, $(g^{\text{MAIM2}})_1(\omega)$, $(g^{\text{MAIM3}})_1(\omega)$, $(g^{\text{MAIM4}})_1(\omega)$ and $(g^{\text{AIM}})_1(\omega; 4, 2, 1e4)$ for $d_1 = 0.6$ for linear advection equation (19) with initial condition (20).

As $k = 2n, n \in \mathbb{N}^+$, we can rewrite the requirement above as $k \geq k_{(2n)}^{\text{MAIM}}$ by introducing

$$k_{(2n)}^{\text{MAIM}} = \left\lceil \frac{r}{r-1-n_{\text{cp}}} - 1 \right\rceil + \frac{1 - (-1)^{\left\lceil \frac{r}{r-1-n_{\text{cp}}} - 1 \right\rceil}}{2}.$$

(2) If $k = 2n - 1, n \in \mathbb{N}^+$, from Theorem 1, Corollary 1 and Corollary 2, we have $(g^{\text{MAIM}i})_s(d_s) = d_s$ and $(g^{\text{MAIM}i})'_s(d_s) = (g^{\text{MAIM}i})''_s(d_s) = \dots = (g^{\text{MAIM}i})^{(k+1)}_s(d_s) = 0, (g^{\text{MAIM}i})^{(k+2)}_s(d_s) \neq 0$. Therefore, similarly, evaluation at ω_s^{JS} of the Taylor series approximation of the $(g^{\text{MAIM}i})_s(\omega)$ about d_s yields

$$\begin{aligned} \alpha_s^{\text{MAIM}i} &= (g^{\text{MAIM}i})_s(d_s) + \sum_{l=1}^{k+1} \frac{(g^{\text{MAIM}i})^{(l)}_s(d_s)}{l!} (\omega_s^{\text{JS}} - d_s)^l + \frac{(g^{\text{MAIM}i})^{(k+2)}_s(d_s)}{(k+2)!} (\omega_s^{\text{JS}} - d_s)^{k+2} + \dots \\ &= d_s + \frac{(g^{\text{MAIM}i})^{(k+2)}_s(d_s)}{(k+2)!} (\omega_s^{\text{JS}} - d_s)^{k+2} + \dots \end{aligned}$$

Furthermore, according to Lemma 5 and Lemma 6, the $(2r - 1)$ -th-order WENO-MAIM i schemes can achieve the

optimal $(2r - 1)$ th-order of accuracy with requirement

$$(r - 1 - n_{\text{cp}})(k + 2) \geq r, \quad 1 \leq n_{\text{cp}} < r - 1.$$

As $k = 2n - 1, n \in \mathbb{N}^+$, we can rewrite the requirement above as $k \geq k_{(2n-1)}^{\text{MAIM}}$ by introducing

$$k_{(2n-1)}^{\text{MAIM}} = \left\lceil \frac{r}{r - 1 - n_{\text{cp}}} - 2 \right\rceil + \frac{1 + (-1)^{\left\lfloor \frac{r}{r - 1 - n_{\text{cp}}} - 2 \right\rfloor}}{2}.$$

Clearly, we only need to ensure $k \geq k^{\text{MAIM}}$, with $k^{\text{MAIM}} = \min(k_{(2n-1)}^{\text{MAIM}}, k_{(2n)}^{\text{MAIM}})$, to achieve the optimal $(2r - 1)$ th-order of accuracy. It is easy to check that $k_{(2n-1)}^{\text{MAIM}} \leq k_{(2n)}^{\text{MAIM}}$. Eventually, we obtain

$$k^{\text{MAIM}} = \left\lceil \frac{r}{r - 1 - n_{\text{cp}}} - 2 \right\rceil + \frac{1 + (-1)^{\left\lfloor \frac{r}{r - 1 - n_{\text{cp}}} - 2 \right\rfloor}}{2}. \quad (23)$$

□

Remark 5. For different values of n_{cp} , we can calculate the detailed convergence order of the WENO-MAIMi schemes using Theorem 2. Table 1 is a comparison between WENO-JS, WENO-M(1), WENO-M(2), WENO-IM(k, A) and WENO-MAIMi. Note that WENO-M(n) stands for WENO-M schemes with n times mapping, and their rates of convergence are related to r and n_{cp} . A general conclusion of the rates of convergence of WENO-M(n) schemes is proposed in Lemma 7, and we provide the proof in Appendix B.

Lemma 7. If n mapping is used in the $(2r - 1)$ th-order WENO-M scheme, then for different values of n_{cp} , the weights ω_s^{M} in the $(2r - 1)$ th-order WENO-M scheme satisfy

$$\omega_s^{\text{M}} - d_s = O((\Delta x)^{3^n \times (r-1-n_{\text{cp}})}), \quad r = 2, 3, \dots, 9, \quad n_{\text{cp}} = 0, 1, \dots, r - 1,$$

and the rate of convergence is

$$r_c = \begin{cases} 2r - 1, & \text{if } n_{\text{cp}} = 0, \dots, \left\lfloor \frac{3^n - 1}{3^n} r - 1 \right\rfloor, \\ (3^n + 1)(r - 1) - 3^n \times n_{\text{cp}}, & \text{if } n_{\text{cp}} = \left\lfloor \frac{3^n - 1}{3^n} r - 1 \right\rfloor + 1, \dots, r - 1. \end{cases}$$

where $\lfloor x \rfloor$ is a floor function of x .

4. Numerical experiments

In this section, we present the results of the modified adaptive improved mapped WENO-MAIMi schemes in comparison with WENO-JS, WENO-M, WENO-PM6 and WENO-IM(2, 0.1), and all these schemes are in the finite volume version with $\epsilon = 10^{-40}$. The global Lax-Friedrichs numerical flux is used in the following numerical experiments. The L_1 norm of the error is calculated by comparing the numerical solution $(u_h)_j$ with the exact solution u_j^{exact} according to

$$L_1(h) = \sum_j h \cdot |u_j^{\text{exact}} - (u_h)_j|.$$

where $h = \Delta x$ is the spatial step size.

Now, we focus on the performance of fifth-order WENO-MAIM1($k = 10, A = 1e-6, m_s = 0.06$), WENO-MAIM2($k = 2, A = 0.1, Q = 10, \text{CFS}_s = 1e-6$), WENO-MAIM3($k = 10, A = 1e-6$) and WENO-MAIM4($k =$

1.0, $A = 1e-6$). Notably, the main purpose for choosing the specific WENO-MAIM2($k = 2, A = 0.1, Q = 10, CFS_s = 1e-6$) here is to verify the conclusion in subsection 3.4.2 that WENO-MAIM2($k, A, Q, CFS_s = 0$) = WENO-IM(k, A) by means of numerical examples. We show that for all the following examples, WENO-MAIM2($k = 2, A = 0.1, Q = 10, CFS_s = 1e-6$) provides exactly the same results as WENO-IM(2, 0.1). Without causing any confusion, we denote these four schemes as WENO-MAIM1, WENO-MAIM2, WENO-MAIM3 and WENO-MAIM4 for simplicity.

Table 1. Convergence orders for WENO-JS, WENO-M(1), WENO-M(2), WENO-IM(k, A) and WENO-MAIM i .

| | n_{sp} | r_c -WENO-JS | r_c -WENO-M(1) | r_c -WENO-M(2) | r_c -WENO-IM(k, A) | r_c -WENO-MAIM i |
|---------|----------|----------------|------------------|------------------|--------------------------|----------------------|
| $r = 2$ | 0 | 3 | 3 | 3 | $3(k \geq 2)$ | $3(k \geq 1)$ |
| | 1 | 1 | 1 | 1 | 1 | 1 |
| $r = 3$ | 0 | 5 | 5 | 5 | $5(k \geq 2)$ | $5(k \geq 1)$ |
| | 1 | 3 | 5 | 5 | $5(k \geq 2)$ | $5(k \geq 1)$ |
| | 2 | 2 | 2 | 2 | 2 | 2 |
| $r = 4$ | 0 | 7 | 7 | 7 | $7(k \geq 2)$ | $7(k \geq 1)$ |
| | 1 | 5 | 7 | 7 | $7(k \geq 2)$ | $7(k \geq 1)$ |
| | 2 | 4 | 6 | 7 | $7(k \geq 4)$ | $7(k \geq 3)$ |
| | 3 | 3 | 3 | 3 | 3 | 3 |
| $r = 5$ | 0 | 9 | 9 | 9 | $9(k \geq 2)$ | $9(k \geq 1)$ |
| | 1 | 7 | 9 | 9 | $9(k \geq 2)$ | $9(k \geq 1)$ |
| | 2 | 6 | 9 | 9 | $9(k \geq 2)$ | $9(k \geq 1)$ |
| | 3 | 5 | 7 | 9 | $9(k \geq 4)$ | $9(k \geq 3)$ |
| | 4 | 4 | 4 | 4 | 4 | 4 |
| $r = 6$ | 0 | 11 | 11 | 11 | $11(k \geq 2)$ | $11(k \geq 1)$ |
| | 1 | 9 | 11 | 11 | $11(k \geq 2)$ | $11(k \geq 1)$ |
| | 2 | 8 | 11 | 11 | $11(k \geq 2)$ | $11(k \geq 1)$ |
| | 3 | 7 | 11 | 11 | $11(k \geq 2)$ | $11(k \geq 1)$ |
| | 4 | 6 | 8 | 11 | $11(k \geq 6)$ | $11(k \geq 5)$ |
| | 5 | 5 | 5 | 5 | 5 | 5 |
| $r = 7$ | 0 | 13 | 13 | 13 | $13(k \geq 2)$ | $13(k \geq 1)$ |
| | 1 | 11 | 13 | 13 | $13(k \geq 2)$ | $13(k \geq 1)$ |
| | 2 | 10 | 13 | 13 | $13(k \geq 2)$ | $13(k \geq 1)$ |
| | 3 | 9 | 13 | 13 | $13(k \geq 2)$ | $13(k \geq 1)$ |
| | 4 | 8 | 12 | 13 | $13(k \geq 4)$ | $13(k \geq 3)$ |
| | 5 | 7 | 9 | 13 | $13(k \geq 6)$ | $13(k \geq 5)$ |
| | 6 | 6 | 6 | 6 | 6 | 6 |
| $r = 8$ | 0 | 15 | 15 | 15 | $15(k \geq 2)$ | $15(k \geq 1)$ |
| | 1 | 13 | 15 | 15 | $15(k \geq 2)$ | $15(k \geq 1)$ |
| | 2 | 12 | 15 | 15 | $15(k \geq 2)$ | $15(k \geq 1)$ |
| | 3 | 11 | 15 | 15 | $15(k \geq 2)$ | $15(k \geq 1)$ |
| | 4 | 10 | 15 | 15 | $15(k \geq 2)$ | $15(k \geq 1)$ |
| | 5 | 9 | 13 | 15 | $15(k \geq 4)$ | $15(k \geq 3)$ |
| | 6 | 8 | 10 | 15 | $15(k \geq 8)$ | $15(k \geq 7)$ |
| | 7 | 7 | 7 | 7 | 7 | 7 |
| $r = 9$ | 0 | 17 | 17 | 17 | $17(k \geq 2)$ | $17(k \geq 1)$ |
| | 1 | 15 | 17 | 17 | $17(k \geq 2)$ | $17(k \geq 1)$ |
| | 2 | 14 | 17 | 17 | $17(k \geq 2)$ | $17(k \geq 1)$ |
| | 3 | 13 | 17 | 17 | $17(k \geq 2)$ | $17(k \geq 1)$ |
| | 4 | 12 | 17 | 17 | $17(k \geq 2)$ | $17(k \geq 1)$ |
| | 5 | 11 | 17 | 17 | $17(k \geq 2)$ | $17(k \geq 1)$ |
| | 6 | 10 | 14 | 17 | $17(k \geq 4)$ | $17(k \geq 3)$ |
| | 7 | 9 | 11 | 17 | $17(k \geq 8)$ | $17(k \geq 7)$ |
| | 8 | 8 | 8 | 8 | 8 | 8 |

4.1. The linear advection problem

Example 1. (Accuracy test without any critical points [8]) We solve the one-dimensional linear advection equation $u_t + u_x = 0$ with the following initial condition

$$u(x, 0) = \sin(\pi x) \quad (24)$$

and the periodic boundary conditions. Note that we consider only the fifth-order methods here, and to ensure that the error for the overall scheme is a measure of the spatial convergence only, we set the CFL number to be $(\Delta x)^{2/3}$. Clearly, the initial condition in (24) has no critical points.

The errors and convergence rates for the numerical solutions of Example 1 produced by various schemes in the L_1 norm at output time $t = 2.0$ are shown in Table 2. All the schemes achieve close to their designed order of accuracy. In terms of accuracy, WENO-MAIM1, WENO-MAIM2, WENO-MAIM3 and WENO-MAIM4 provide

Table 2. Convergence properties of various schemes solving $u_t + u_x = 0$ with initial condition $u(x, 0) = \sin(\pi x)$.

| N | 20 | 40 | 80 | 160 | 320 |
|----------------|----------------|---------------------|---------------------|---------------------|---------------------|
| WENO-JS | 2.96529e-03(-) | 9.27609e-05(4.9985) | 2.89265e-06(5.0031) | 9.03392e-08(5.0009) | 2.82330e-09(4.9999) |
| WENO-M | 5.18291e-04(-) | 1.59422e-05(5.0288) | 4.98914e-07(4.9979) | 1.56021e-08(4.9990) | 4.88356e-10(4.9977) |
| WENO-PM6 | 5.02923e-04(-) | 1.59130e-05(4.9821) | 4.98858e-07(4.9954) | 1.56020e-08(4.9988) | 4.88355e-10(4.9977) |
| WENO-IM(2,0.1) | 5.04401e-04(-) | 1.59160e-05(4.9860) | 4.98863e-07(4.9957) | 1.56020e-08(4.9988) | 4.88355e-10(4.9977) |
| WENO-MAIM1 | 5.08205e-04(-) | 1.59130e-05(4.9971) | 4.98858e-07(4.9954) | 1.56020e-08(4.9988) | 4.88355e-10(4.9977) |
| WENO-MAIM2 | 5.04401e-04(-) | 1.59160e-05(4.9860) | 4.98863e-07(4.9957) | 1.56020e-08(4.9988) | 4.88355e-10(4.9977) |
| WENO-MAIM3 | 5.02844e-04(-) | 1.59130e-05(4.9818) | 4.98858e-07(4.9954) | 1.56020e-08(4.9988) | 4.88355e-10(4.9977) |
| WENO-MAIM4 | 5.02845e-04(-) | 1.59131e-05(4.9818) | 4.98858e-07(4.9954) | 1.56020e-08(4.9988) | 4.88355e-10(4.9977) |

almost equally accurate numerical solutions as WENO-PM6 and WENO-IM(2, 0.1), which provide more accurate numerical solutions than WENO-JS and WENO-M.

Example 2. (Accuracy test with first-order critical points [16]) We solve the one-dimensional linear advection equation $u_t + u_x = 0$ with the following initial condition

$$u(x, 0) = \sin\left(\pi x - \frac{\sin(\pi x)}{\pi}\right) \quad (25)$$

and periodic boundary conditions. Again, the CFL number is set to be $(\Delta x)^{2/3}$. It is easy to verify that the particular initial condition (25) has two first-order critical points, which all have a non-vanishing third derivative.

The errors and convergence rates for the numerical solutions of Example 2 produced by various schemes in the L_1 norm at output time $t = 2.0$ are shown in Table 3. From Table 3, we can observe that WENO-MAIM1, WENO-MAIM2, WENO-MAIM3 and WENO-MAIM4 maintain the fifth-order convergence rate even in the presence of critical points. Moreover, in terms of accuracy, these four WENO schemes provide the equally accurate results as WENO-M, WENO-PM6 and WENO-IM(2, 0.1), and are much more accurate than WENO-JS, whose error is much worse and lower than fifth-order, as shown in Table 3.

Table 3. Convergence properties of various schemes solving $u_t + u_x = 0$ with initial condition $u(x, 0) = \sin(\pi x - \sin(\pi x)/\pi)$.

| N | 20 | 40 | 80 | 160 | 320 |
|----------------|----------------|---------------------|---------------------|---------------------|---------------------|
| WENO-JS | 1.01260e-02(-) | 7.22169e-04(3.8096) | 3.42286e-05(4.3991) | 1.58510e-06(4.4326) | 7.95517e-08(4.3165) |
| WENO-M | 3.70838e-03(-) | 1.45082e-04(4.6758) | 4.80253e-06(4.9169) | 1.52120e-07(4.9805) | 4.77083e-09(4.9948) |
| WENO-PM6 | 4.82173e-03(-) | 1.55428e-04(4.9952) | 4.87327e-06(4.9952) | 1.52750e-07(4.9956) | 4.77729e-09(4.9988) |
| WENO-IM(2,0.1) | 4.30725e-03(-) | 1.51327e-04(4.8310) | 4.85592e-06(4.9618) | 1.52659e-07(4.9914) | 4.77654e-09(4.9982) |
| WENO-MAIM1 | 8.07923e-03(-) | 3.32483e-04(4.6029) | 1.01162e-05(5.0385) | 1.52910e-07(6.0478) | 4.77728e-09(5.0003) |
| WENO-MAIM2 | 4.30725e-03(-) | 1.51327e-04(4.8310) | 4.85592e-06(4.9618) | 1.52659e-07(4.9914) | 4.77654e-09(4.9982) |
| WENO-MAIM3 | 4.39527e-03(-) | 1.52219e-04(4.8517) | 4.86436e-06(4.9678) | 1.52735e-07(4.9931) | 4.77728e-09(4.9987) |
| WENO-MAIM4 | 4.94421e-03(-) | 1.52224e-04(5.0215) | 4.86436e-06(4.9678) | 1.52735e-07(4.9931) | 4.77728e-09(4.9987) |

Example 3. (Non-/Oscillatory test with long output time [7, 8]) We solve the one-dimensional linear advection equation $u_t + u_x = 0$ with the following initial condition

$$u(x, 0) = \begin{cases} \frac{1}{6}[G(x, \beta, z - \hat{\delta}) + 4G(x, \beta, z) + G(x, \beta, z + \hat{\delta})], & x \in [-0.8, -0.6], \\ 1, & x \in [-0.4, -0.2], \\ 1 - |10(x - 0.1)|, & x \in [0.0, 0.2], \\ \frac{1}{6}[F(x, \alpha, a - \hat{\delta}) + 4F(x, \alpha, a) + F(x, \alpha, a + \hat{\delta})], & x \in [0.4, 0.6], \\ 0, & \text{otherwise,} \end{cases} \quad (26)$$

where $G(x, \beta, z) = e^{-\beta(x-z)^2}$, $F(x, \alpha, a) = \sqrt{\max(1 - \alpha^2(x-a)^2, 0)}$, and the constants are $z = -0.7$, $\hat{\delta} = 0.005$, $\beta = \frac{\log 2}{36\hat{\delta}^2}$, $a = 0.5$ and $\alpha = 10$. The periodic boundary conditions are used in the two directions and the CFL number is set to be 0.1. This example is obtained from [18] and it consists of a Gaussian, a square wave, a sharp triangle and a semi-ellipse.

Table 4 shows the errors and convergence rates for the numerical solutions of Example 3 produced by various schemes in the L_1 norm at output times $t = 2$ and $t = 2000$. From Table 4, we find the following results: (1) at output time $t = 2$, for all schemes, the L_1 orders are approximately 1.0; (2) at output time $t = 2000$, the L_1 orders decrease to very small values, even negative for the WENO-JS and WENO-M schemes, however, for WENO-PM6, WENO-IM(2, 0.1), WENO-MAIM1, WENO-MAIM2, WENO-MAIM3 and WENO-MAIM4, their L_1 orders are maintained at approximately 1.0. Overall, WENO-MAIM1, WENO-MAIM2, WENO-MAIM3 and WENO-MAIM4 perform as well as WENO-PM6 and WENO-IM(2, 0.1) for this problem with various discontinuities at both short and long output times.

We illustrate the performance of various schemes at output time $t = 2000$ on the mesh $N = 800$ cells in Fig.5. With the exception of WENO-JS and WENO-M, all the other schemes show comparable performances in capturing the Gaussian, square and triangle waves. WENO-PM6, WENO-MAIM1, WENO-MAIM3, WENO-MAIM4 give the highest resolution of the Gaussian but WENO-PM6 generates a small oscillation when x is between 0.6 and 0.7, as shown in Fig.5(a)(c). WENO-IM(2, 0.1), WENO-MAIM1, WENO-MAIM2, WENO-MAIM3, WENO-MAIM4 don't generate any oscillations but WENO-IM(2, 0.1) and WENO-MAIM2 give significantly lower resolutions of the Gaussian. In other words, WENO-MAIM1, WENO-MAIM3 and WENO-MAIM4 follow the exact solution more closely than WENO-IM(2, 0.1) and WENO-MAIM2 for the Gaussian, as shown in Fig.5(a)(b).

Table 4. Convergence properties of various schemes solving $u_t + u_x = 0$ with initial condition Eq.(26).

| N | $t = 2$ | | | $t = 2000$ | | |
|----------------|----------------|---------------------|----------------------|----------------|---------------------|-----------------------|
| | 200 | 400 | 800 | 200 | 400 | 800 |
| WENO-JS | 6.30497e-02(-) | 2.81654e-02(1.1626) | 1.41364e-02 (0.9945) | 6.12899e-01(-) | 5.99215e-01(0.0326) | 5.50158e-01 (0.1232) |
| WENO-M | 4.77201e-02(-) | 2.23407e-02(1.0949) | 1.11758e-02 (0.9993) | 3.81597e-01(-) | 3.25323e-01(0.2302) | 3.48528e-01 (-0.0994) |
| WENO-PM6 | 4.66681e-02(-) | 2.13883e-02(1.1256) | 1.06477e-02 (1.0063) | 2.17323e-01(-) | 1.05197e-01(1.0467) | 4.47703e-02 (1.2325) |
| WENO-IM(2,0.1) | 4.40293e-02(-) | 2.02331e-02(1.1217) | 1.01805e-02 (0.9909) | 2.17411e-01(-) | 1.12590e-01(0.9493) | 5.18367e-02 (1.1190) |
| WENO-MAIM1 | 5.71142e-02(-) | 2.48065e-02(1.2031) | 1.21078e-02 (1.0348) | 2.18238e-01(-) | 1.09902e-01(0.9897) | 4.41601e-02 (1.3154) |
| WENO-MAIM2 | 4.40293e-02(-) | 2.02331e-02(1.1217) | 1.01805e-02 (0.9909) | 2.17411e-01(-) | 1.12590e-01(0.9493) | 5.18367e-02 (1.1190) |
| WENO-MAIM3 | 4.61945e-02(-) | 2.12930e-02(1.1173) | 1.05994e-02 (1.0064) | 2.17339e-01(-) | 9.91687e-02(1.1320) | 4.37214e-02 (1.1815) |
| WENO-MAIM4 | 5.02152e-02(-) | 2.36585e-02(1.0858) | 1.16751e-02 (1.0189) | 2.18548e-01(-) | 1.03499e-01(1.0783) | 4.39609e-02 (1.2353) |

4.2. One-dimensional Euler system

In this subsection, we present numerical examples of the one-dimensional Euler system for gas dynamics with different initial and boundary conditions in the following conservation form

$$\mathbf{U}_t + \mathbf{F}(\mathbf{U})_x = 0, \quad (27)$$

where $\mathbf{U} = (\rho, \rho u, E)^T$, $\mathbf{F}(\mathbf{U}) = (\rho u, \rho u^2 + p, u(E + p))^T$, and ρ, u, p and E are the density, velocity, pressure and total energy, respectively. The Euler system (27) is closed by the equation of state for an ideal polytropic gas, which is given by

$$p = (\gamma - 1)\left(E - \frac{1}{2}\rho u^2\right), \quad \gamma = 1.4$$

The finite volume version of the characteristic-wise one-dimensional WENO procedure is employed, and we refer to [21] for details. In all calculations, the CFL number is set to be 0.1 unless it is specified and the reference solutions are obtained by using WENO-JS at the resolution $N = 10000$ cells.

Example 4. (Sod's shock tube problem [24]) We solve the Euler system (27) with the transmissive boundary conditions in two directions and the following initial conditions

$$(\rho, u, p)(x, 0) = \begin{cases} (1.0, 0.0, 1.0), & x \in [0.0, 0.5], \\ (0.125, 0.0, 0.1), & x \in [0.5, 1.0]. \end{cases} \quad (28)$$

Fig.6 shows the density computed by WENO-JS, WENO-M, WENO-PM6, WENO-IM(2, 0.1) and WENO-MAIM i ($i = 1, 2, 3, 4$) at $t = 0.25$ with the cell number $N = 200$. From Fig.6, we observe that all the mapped schemes perform better than the WENO-JS scheme at the contact discontinuity and shock. Close examinations show that WENO-MAIM2 and WENO-IM(2, 0.1) capture very slightly sharper contact discontinuity and shock compared to WENO-MAIM3, and then WENO-MAIM4, WENO-M, WENO-PM6, WENO-MAIM1 followed.

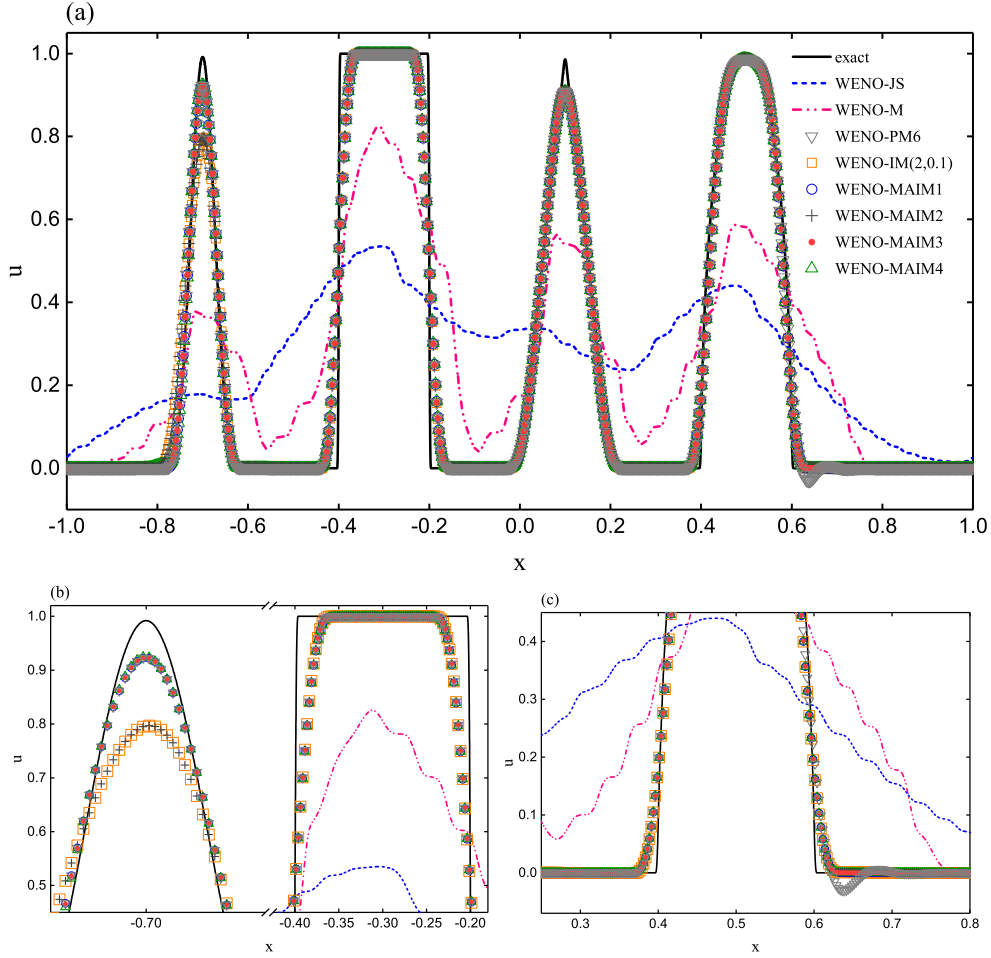


Fig. 5. Performance of the fifth-order WENO-JS, WENO-M, WENO-PM6, WENO-IM(2,0.1) and WENO-MAIM i ($i = 1, 2, 3, 4$) schemes for linear advection $u_t + u_x = 0$ with initial condition (26).

Example 5. (Shu-Osher shock-entropy wave interaction problem [23]) We solve the one-dimensional shock-entropy wave interaction problem with the transmissive boundary conditions in two directions specified by the following initial conditions

$$(\rho, u, p)(x, 0) = \begin{cases} (3.857143, 2.629369, 10.333333), & x \in [-5.0, -4.0], \\ (1.0 + 0.2 \sin(5x), 0, 1), & x \in [-4.0, 5.0]. \end{cases} \quad (29)$$

Fig.7 shows the density computed by WENO-JS, WENO-M, WENO-PM6, WENO-IM(2,0.1) and WENO-MAIM i ($i = 1, 2, 3, 4$) at $t = 1.8$ with the cell number $N = 300$. It is clear from the results in Fig.7 that, among all the schemes, WENO-JS is the most dissipative one followed by WENO-MAIM1. WENO-MAIM2, WENO-MAIM3 and WENO-IM(2,0.1) produce the largest amplitudes of the short wavelength oscillations and WENO-MAIM4, WENO-M, WENO-PM6 also show comparable performances in capturing these oscillations.

Example 6. (Titarev-Toro shock-entropy wave interaction problem [25, 27, 26]) We solve a more severe version of Example 5 specified by the following initial conditions

$$(\rho, u, p)(x, 0) = \begin{cases} (1.515695, 0.5233346, 1.80500), & x \in [-5.0, -4.5], \\ (1.0 + 0.1 \sin(20\pi x), 0, 1), & x \in [-4.5, 5.0]. \end{cases} \quad (30)$$

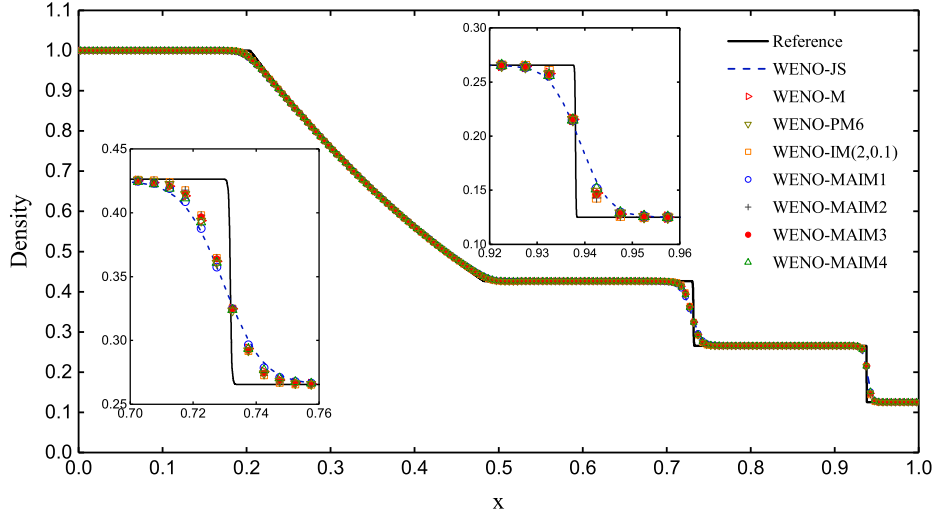


Fig. 6. Performance of fifth-order WENO-JS, WENO-M, WENO-PM6, WENO-IM(2, 0.1) and WENO-MAIM i ($i = 1, 2, 3, 4$) for Euler system (27) with initial condition (28).

This problem produces waves of shorter wavelength compared to Example 5. It was run with $N = 1500$ uniform cells till $t = 5.0$ and the CFL number is set to be 0.4.

The results are shown in Fig.8. It can be seen that WENO-MAIM3 results in slightly greater amplitudes compared to WENO-MAIM2, WENO-MAIM4 and WENO-IM(2, 0.1), which produce higher amplitudes of the short wavelength oscillations compared to WENO-M and WENO-PM6. WENO-JS was found to perform worse than all the mapped WENO schemes for this case and WENO-MAIM1 performs slightly better than WENO-JS.

Example 7. (Woodward-Colella interacting blast wave problem [30]) We solve the one-dimensional blast waves interaction problem of Woodward and Colella, which has the following initial condition with reflective boundary conditions

$$(\rho, u, p)(x, 0) = \begin{cases} (1, 0, 1000), & x \in [0, 0.1), \\ (1, 0, 0.01), & x \in [0.1, 0.9), \\ (1, 0, 100), & x \in [0.9, 1.0]. \end{cases} \quad (31)$$

This problem was run with $N = 400$ uniform cells till $t = 0.038$ by WENO-JS, WENO-M, WENO-PM6, WENO-IM(2, 0.1) and WENO-MAIM i ($i = 1, 2, 3, 4$).

Surprisingly, for this specific problem, WENO-MAIM2 and WENO-IM(2, 0.1) blow up in our calculations, but the other schemes perform well. The results are given in Fig.9. It can be observed directly from Fig.9 that WENO-MAIM3 provides the best performance, followed by WENO-MAIM4, WENO-M and WENO-PM6. WENO-MAIM1 performs worse than most of the schemes but slightly better than WENO-JS.

Example 8. (123 problem [28, 4]) We solve the 123 problem with the following initial condition and transmissive boundary conditions

$$(\rho, u, p)(x, 0) = \begin{cases} (1, -2, 0.4), & x \in [0, 0.5), \\ (1, 2, 0.4), & x \in [0.5, 1.0]. \end{cases} \quad (32)$$

This problem was run with $N = 400$ uniform cells till $t = 0.15$ by WENO-JS, WENO-M, WENO-PM6, WENO-IM(2, 0.1) and WENO-MAIM i ($i = 1, 2, 3, 4$).

All these schemes perform well in this severe problem and the results are given in Fig.10. Fig.10(b) indicates that WENO-MAIM2 and WENO-IM(2, 0.1) provide the best performance, followed by WENO-MAIM3.

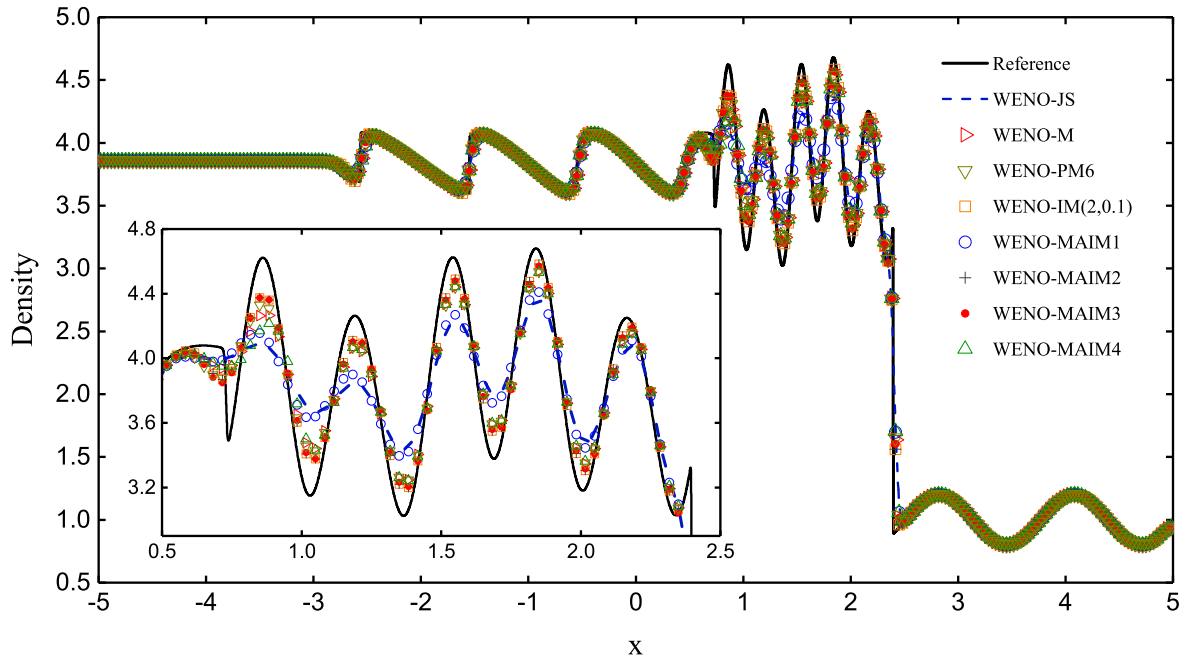


Fig. 7. Performance of fifth-order WENO-JS, WENO-M, WENO-PM6, WENO-IM(2, 0.1) and WENO-MAIM i ($i = 1, 2, 3, 4$) for Euler system (27) with initial condition (29).

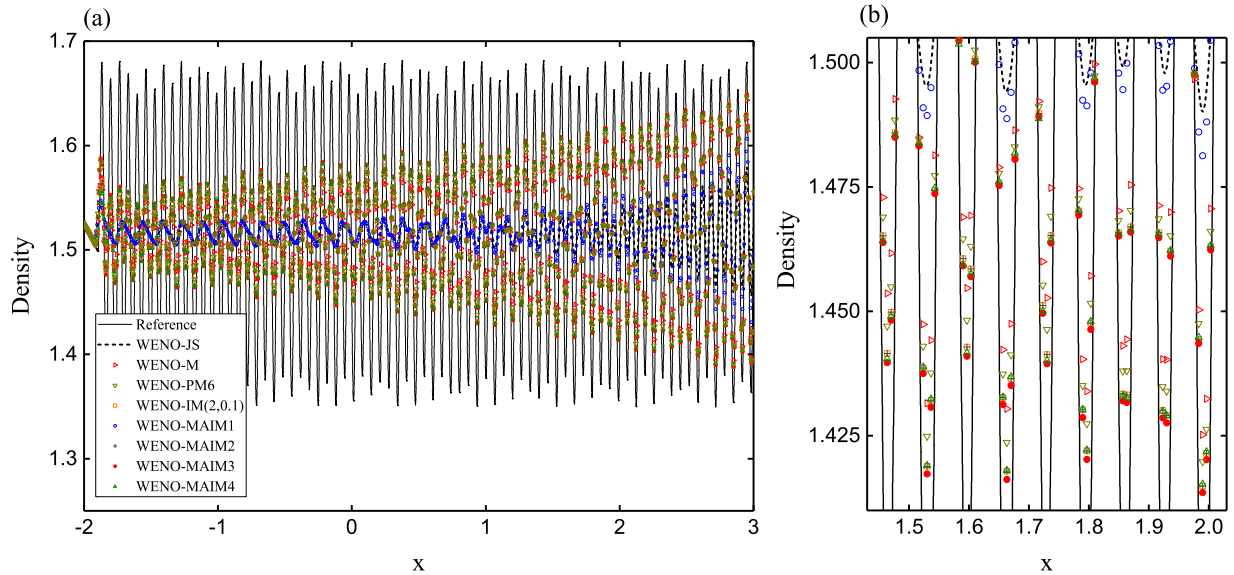


Fig. 8. Performance of fifth-order WENO-JS, WENO-M, WENO-PM6, WENO-IM(2, 0.1) and WENO-MAIM i ($i = 1, 2, 3, 4$) for Euler system (27) with initial condition (30).

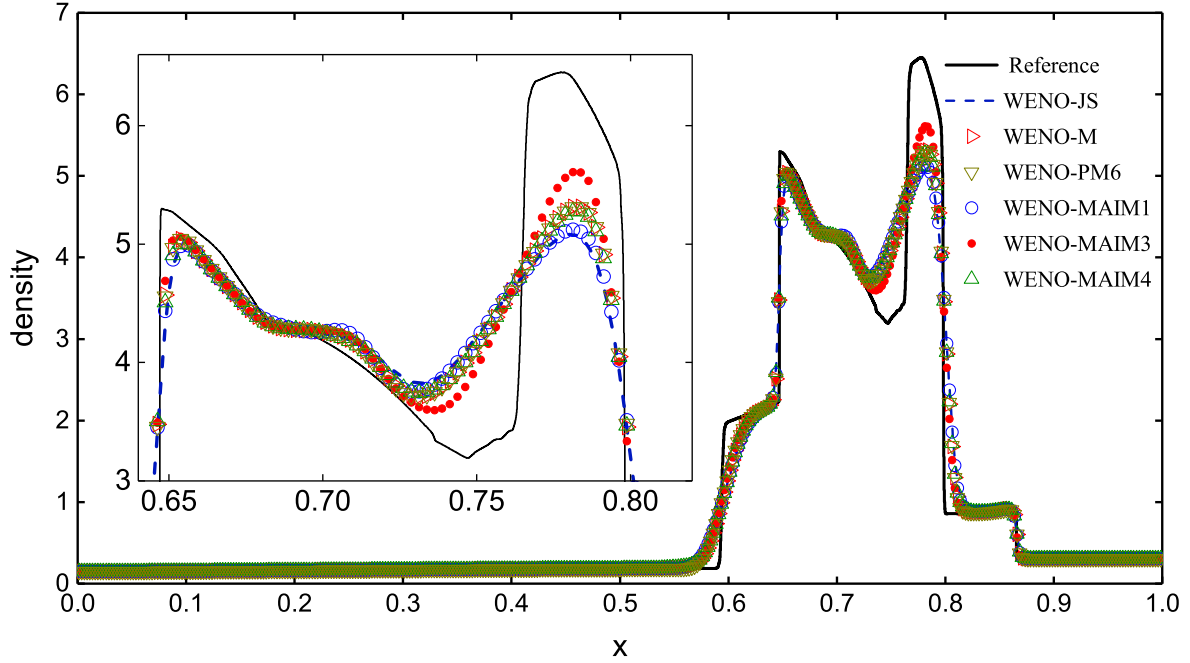


Fig. 9. Performance of fifth-order WENO-JS, WENO-M, WENO-PM6 and WENO-MAIM i ($i = 1, 3, 4$) for Euler system (27) with initial condition (31).

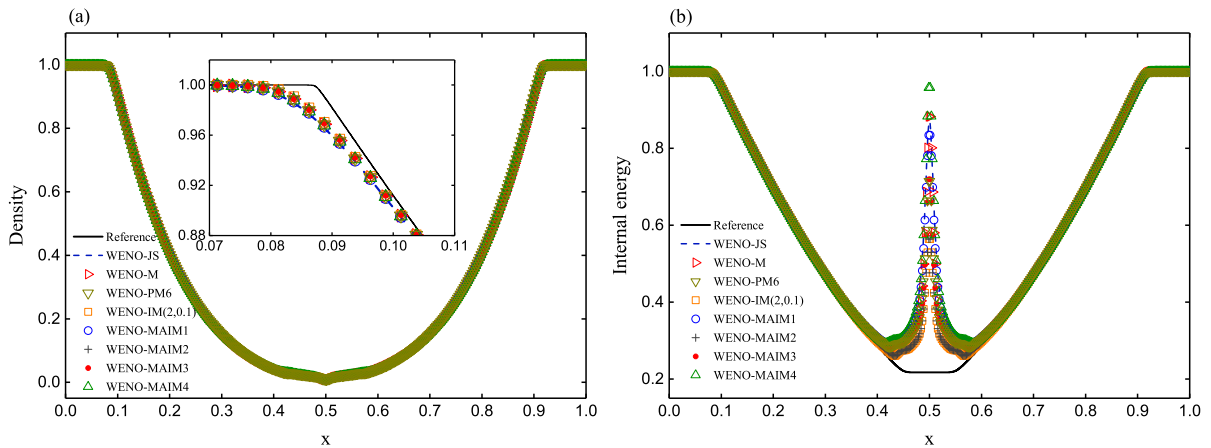


Fig. 10. Performance of fifth-order WENO-JS, WENO-M, WENO-PM6, WENO-IM(2, 0.1) and WENO-MAIM i ($i = 1, 2, 3, 4$) for Euler system (27) with initial condition (32).

5. Conclusions

We proposed a modified adaptive improved mapped WENO method by employing new mapping functions. The new mapping functions are based on some adaptive control functions and a smoothing approximation of the signum function. This helps to provide a wider selection of parameter in the schemes, and exhibits some improved comprehensive performance in numerical experiments. Four WENO-MAIM i schemes are our recommendation in most hyperbolic conservation simulations, especially for long output time cases, and the WENO-MAIM3 scheme with parameters as $k = 10$, $A = 1e-6$ may be the best choice.

Appendix A

The objective of this appendix is to present the results of the zero points of $q'_s(\omega)$, the monotone intervals and maximum values of $q_s(\omega)$ in $\omega \in (0, 1)$, and the recommended values of α_s in Property 3 and Property 4 for various $(2r - 1)$ th-order WENO schemes (see Table 5).

Table 5. The results of the zero points of $q'_s(\omega)$, the monotone intervals and maximum values of $q_s(\omega)$ in $\omega \in (0, 1)$, and the recommended values of α_s in Property 3 and Property 4 for various $(2r - 1)$ th-order WENO schemes with $r \in \{1, \dots, 9\}$.

| r | s | d_s | ω_{crit} | $q'_s(\omega)$ | | | $q_{\text{max}}(\omega)$ | recommended value of α_s |
|-----|-----|------------|------------------------|--|---------------------------------|--|--------------------------|---------------------------------|
| | | | | $\omega \in (0, \omega_{\text{crit}})$ | $\omega = \omega_{\text{crit}}$ | $\omega \in (\omega_{\text{crit}}, 1)$ | | |
| 1 | 0 | 1 | - | > 0 | > 0 | > 0 | < 0 | 0.0001 |
| 2 | 0 | 1/3 | 0.380873415 | > 0 | = 0 | < 0 | 0.092362764 | 0.0924 |
| | 1 | 2/3 | 0.619126585 | > 0 | = 0 | < 0 | 0.092362764 | 0.0924 |
| 3 | 0 | 1/10 | 0.156515839 | > 0 | = 0 | < 0 | 0.574903653 | 0.5750 |
| | 1 | 6/10 | 0.570057856 | > 0 | = 0 | < 0 | 0.033129692 | 0.0332 |
| | 2 | 3/10 | 0.354983613 | > 0 | = 0 | < 0 | 0.133395837 | 0.1334 |
| 4 | 0 | 1/35 | 0.050334141 | > 0 | = 0 | < 0 | 0.954367890 | 0.9544 |
| | 1 | 12/35 | 0.388078022 | > 0 | = 0 | < 0 | 0.082052483 | 0.0821 |
| | 2 | 18/35 | 0.509902230 | > 0 | = 0 | < 0 | 0.000674949 | 0.0007 |
| | 3 | 4/35 | 0.174716514 | > 0 | = 0 | < 0 | 0.527277883 | 0.5273 |
| 5 | 0 | 1/126 | 0.014533733 | > 0 | = 0 | < 0 | 1.289877215 | 1.2899 |
| | 1 | 10/63 | 0.226106436 | > 0 | = 0 | < 0 | 0.401303129 | 0.4014 |
| | 2 | 10/21 | 0.483489850 | > 0 | = 0 | < 0 | 0.001874973 | 0.0019 |
| | 3 | 20/63 | 0.368684520 | > 0 | = 0 | < 0 | 0.110936397 | 0.1110 |
| | 4 | 5/126 | 0.068631349 | > 0 | = 0 | < 0 | 0.862927630 | 0.8630 |
| 6 | 0 | 1/462 | 0.004036768 | > 0 | = 0 | < 0 | 1.617654227 | 1.6177 |
| | 1 | 5/77 | 0.107726908 | > 0 | = 0 | < 0 | 0.716954249 | 0.7170 |
| | 2 | 25/77 | 0.374254393 | > 0 | = 0 | < 0 | 0.102277562 | 0.1023 |
| | 3 | 100/231 | 0.453273191 | > 0 | = 0 | < 0 | 0.014901369 | 0.0150 |
| | 4 | 25/154 | 0.229973747 | > 0 | = 0 | < 0 | 0.392223085 | 0.3923 |
| | 5 | 1/77 | 0.023524596 | > 0 | = 0 | < 0 | 1.163386235 | 1.1634 |
| 7 | 0 | 1/1716 | 0.001099119 | > 0 | = 0 | < 0 | 1.945668808 | 1.9457 |
| | 1 | 7/286 | 0.043419023 | > 0 | = 0 | < 0 | 0.996333645 | 0.9964 |
| | 2 | 105/572 | 0.251943992 | > 0 | = 0 | < 0 | 0.341617878 | 0.3417 |
| | 3 | 175/429 | 0.435602337 | > 0 | = 0 | < 0 | 0.028078584 | 0.0281 |
| | 4 | 175/572 | 0.359684813 | > 0 | = 0 | < 0 | 0.125509465 | 0.1256 |
| | 5 | 21/286 | 0.120110409 | > 0 | = 0 | < 0 | 0.678155990 | 0.6782 |
| | 6 | 7/1716 | 0.007550349 | > 0 | = 0 | < 0 | 1.458456912 | 1.4585 |
| 8 | 0 | 1/6435 | 0.000295439 | > 0 | = 0 | < 0 | 2.275453190 | 2.2755 |
| | 1 | 56/6435 | 0.015907656 | > 0 | = 0 | < 0 | 1.266360740 | 1.2664 |
| | 2 | 196/2145 | 0.145076866 | > 0 | = 0 | < 0 | 0.605994603 | 0.6060 |
| | 3 | 392/1287 | 0.358612853 | > 0 | = 0 | < 0 | 0.127291552 | 0.1273 |
| | 4 | 490/1287 | 0.416050440 | > 0 | = 0 | < 0 | 0.047165647 | 0.0472 |
| | 5 | 392/2145 | 0.251123145 | > 0 | = 0 | < 0 | 0.343478122 | 0.3435 |
| | 6 | 196/6435 | 0.053489044 | > 0 | = 0 | < 0 | 0.936837253 | 0.9369 |
| | 7 | 8/6435 | 0.002330913 | > 0 | = 0 | < 0 | 1.756424091 | 1.7565 |
| 9 | 0 | 1/24310 | 0.000078677 | > 0 | = 0 | < 0 | 2.607051525 | 2.6071 |
| | 1 | 36/12155 | 0.005504277 | > 0 | = 0 | < 0 | 2.607051528 | 2.6071 |
| | 2 | 504/12155 | 0.071503078 | > 0 | = 0 | < 0 | 0.850403988 | 0.8505 |
| | 3 | 2352/12155 | 0.261799125 | > 0 | = 0 | < 0 | 0.319476358 | 0.3195 |
| | 4 | 882/2431 | 0.402941270 | > 0 | = 0 | < 0 | 0.062457658 | 0.0625 |
| | 5 | 3528/12155 | 0.347184466 | > 0 | = 0 | < 0 | 0.146872875 | 0.1469 |
| | 6 | 1176/12155 | 0.152246813 | > 0 | = 0 | < 0 | 0.586388730 | 0.5864 |
| | 7 | 144/12155 | 0.021508966 | > 0 | = 0 | < 0 | 1.187147894 | 1.1872 |
| | 8 | 9/24310 | 0.000700372 | > 0 | = 0 | < 0 | 2.058883535 | 2.0589 |

Appendix B

In this appendix, we present the proof of Lemma 7.

Proof of Lemma 7.

First, by employing the mapping function Eq.(6), the mapped weights with n times mapping are given by

$$\omega_s^{M(n)} = \frac{\alpha_s^{M(n)}}{\sum_{l=0}^{r-1} \alpha_l^{M(n)}}, \alpha_s^{M(n)} = (g^M)_s(\omega_s^{M(n-1)}), \quad s = 0, 1, \dots, r-1,$$

where $\omega_s^{M(n-1)}$ are the mapped weights with $n-1$ times mapping. Clearly, the mapped weights with 0 times mapping are determined by

$$\omega_s^{M(0)} = \omega_s^{JS}, \quad (33)$$

which are computed by Eq.(5). Similarly, as $(g^M)_s(d_s) = d_s$ and $(g^M)'_s(d_s) = (g^M)''_s(d_s) = 0, (g^M)'''_s(d_s) \neq 0$ in the WENO-M scheme, evaluation at $\omega_s^{M(n-1)}$ of the Taylor series approximations of $(g^M)_s(\omega)$ about d_s yields

$$\begin{aligned} \alpha_s^{M(n)} &= (g^M)_s(d_s) + (g^M)'_s(d_s)(\omega_s^{M(n-1)} - d_s) + \frac{(g^M)''_s(d_s)}{2!}(\omega_s^{M(n-1)} - d_s)^2 + \frac{(g^M)'''_s(d_s)}{3!}(\omega_s^{M(n-1)} - d_s)^3 + \dots \\ &= d_s + \frac{(g^M)'''_s(d_s)}{3!}(\omega_s^{M(n-1)} - d_s)^3 + \dots \end{aligned}$$

By employing the fact that $\sum_{s=0}^{r-1} d_s = 1$, we obtain

$$\frac{1}{\sum_{l=0}^{r-1} \alpha_l^{M(n)}} = 1 + O((\omega_s^{M(n-1)} - d_s)^3).$$

and then,

$$\omega_s^{M(n)} - d_s = O((\omega_s^{M(n-1)} - d_s)^3). \quad (34)$$

As Eq.(34) is a recurrence formula, it is easy to obtain

$$\omega_s^{M(n)} - d_s = O((\omega_s^{M(0)} - d_s)^{3^n}). \quad (35)$$

From Eq.(22)(33)(35), we have

$$\omega_s^{M(n)} - d_s = O((\Delta x)^{3^n \times (r-1-n_{cp})}). \quad (36)$$

Therefore, according to Lemma 6 and Eq.(36), the $(2r-1)$ th-order WENO-M schemes can achieve the optimal order of accuracy, namely, $r_c = 2r-1$, with the requirement

$$3^n \times (r-1-n_{cp}) \geq r,$$

then n_{cp} is limited to $n_{cp} \leq \frac{3^n - 1}{3^n} r - 1$, which we rewrite as

$$n_{cp} = 0, 1, \dots, \left\lfloor \frac{3^n - 1}{3^n} r - 1 \right\rfloor.$$

Now, we consider the convergence order for $n_{cp} > \frac{3^n - 1}{3^n} r - 1$. As the convergence order is $O(\Delta x^{r-1}) \cdot O(\omega_s^{M(n)} - d_s)$, which can be found in the statement of page 549 in [16] or from the proof of Lemma 1 in [8], we obtain

$$r_c = (3^n + 1)(r-1) - 3^n \times n_{cp}, \quad \text{if } n_{cp} = \left\lfloor \frac{3^n - 1}{3^n} r - 1 \right\rfloor + 1, \dots, r-1.$$

□

References

- [1] F. Arandiga, A. Baeza, A.M. Belda, P. Mulet, Analysis of WENO schemes for full and global accuracy, *SIAM J. Numer. Anal.* 49 (2011) 893–915.
- [2] R. Borges, M. Carmona, B. Costa, D.W. S., An improved weighted essentially non-oscillatory scheme for hyperbolic conservation laws, *J. Comput. Phys.* 227 (2008) 3101–3211.
- [3] M. Carmona, B. Costa, D.W. S., High order weighted essentially non-oscillatory WENO-Z schemes for hyperbolic conservation laws, *J. Comput. Phys.* 230 (2011) 1766–1792.
- [4] L. Chen, R. Li, An Integrated Linear Reconstruction for Finite Volume Scheme on Unstructured Grids, *J. Sci. Comput.* 68 (2016) 1172–1197.
- [5] W.S. Don, R. Borges, Accuracy of the weighted essentially non-oscillatory conservative finite difference schemes, *J. Comput. Phys.* 250 (2013) 347–372.
- [6] B. Einfeldt, C.D. Munz, P.L. Roe, B. Sjogreen, On Godunov-Type Methods near Low Densities, *J. Comput. Phys.* 92 (1991) 273–295.
- [7] H. Feng, F. Hu, R. Wang, A new mapped weighted essentially non-oscillatory scheme, *J. Sci. Comput.* 51 (2012) 449–473.
- [8] H. Feng, C. Huang, R. Wang, An improved mapped weighted essentially non-oscillatory scheme, *Appl. Math. Comput.* 232 (2014) 453–468.
- [9] G.A. Gerolymos, D. Senechal, I. Vallet, Very-high-order WENO schemes, *J. Comput. Phys.* 228 (2009) 8481–8524.
- [10] S. Gottlieb, C.W. Shu, Totalvariation diminishing runge-kutta schemes, *Math. Comput.* 67 (1998) 73–85.
- [11] S. Gottlieb, C.W. Shu, E. Tadmor, Strong stability-preserving high-order time discretization methods, *SIAM Rev.* 43 (2001) 89–112.
- [12] A. Harten, ENO schemes with subcell resolution, *J. Comput. Phys.* 83 (1987) 148–184.
- [13] A. Harten, B. Engquist, S. Osher, S. Chakravarthy, Uniformly high order essentially non-oscillatory schemes III, *J. Comput. Phys.* 71 (1987) 231–303.
- [14] A. Harten, B. Osher, S. Engquist, S. Chakravarthy, Some results on uniformly high order accurate essentially non-oscillatory schemes, *Appl. Numer. Math.* 2 (1986) 347–377.
- [15] A. Harten, S. Osher, Uniformly high order essentially non-oscillatory schemes I, *SIAM J. Numer. Anal.* 24 (1987) 279–309.
- [16] A.K. Henrick, T.D. Aslam, J.M. Powers, Mapped weighted essentially non-oscillatory schemes: Achieving optimal order near critical points, *J. Comput. Phys.* 207 (2005) 542–567.
- [17] F. Hu, R. Wang, C. X., A modified fifth-order WENO-Z method hyperbolic conservation laws, *J. Comput. Appl. Math.* 303 (2016) 56–68.
- [18] G.S. Jiang, C.W. Shu, Efficient implementation of weighted ENO schemes, *J. Comput. Phys.* 126 (1996) 202–228.
- [19] Q. Liu, P. Liu, H. Zhang, Piecewise Polynomial Mapping Method and Corresponding WENO Scheme with Improved Resolution, *Commun. Comput. Phys.* 18 (2015) 1417–1444.
- [20] X.D. Liu, S. Osher, T. Chan, Weighted essentially non-oscillatory schemes, *J. Comput. Phys.* 115 (1994) 200–212.
- [21] C.W. Shu, Essentially non-oscillatory and weighted essentially non-oscillatory schemes for hyperbolic conservation laws, in: *Advanced Numerical Approximation of Nonlinear Hyperbolic Equations. Lecture Notes in Mathematics*, volume 1697, Springer, Berlin, 1998, pp. 325–432.
- [22] C.W. Shu, S. Osher, Efficient implementation of essentially non-oscillatory shock-capturing schemes, *J. Comput. Phys.* 77 (1988) 439–471.
- [23] C.W. Shu, S. Osher, Efficient implementation of essentially non-oscillatory shock-capturing schemes II, *J. Comput. Phys.* 83 (1989) 32–78.
- [24] G.A. Sod, A survey of several finite difference methods for systems of nonlinear hyperbolic conservation laws, *J. Comput. Phys.* 107 (1978) 1–31.
- [25] V. Titarev, E. Toro, Finite-volume WENO schemes for three-dimensional conservation laws, *J. Comput. Phys.* 201 (2004) 238–260.
- [26] V. Titarev, E. Toro, WENO schemes based on upwind and centred TVD fluxes, *Comput. Fluids* 34 (2005) 705–720.
- [27] E. Toro, V. Titarev, TVD Fluxes for the High-Order ADER Schemes, *J. Sci. Comput.* 24 (2005) 285–309.
- [28] E.F. Toro, *Riemann Solvers and Numerical Methods for Fluid Dynamics-A Practical Introduction*(Third Edition), Springer, 2009.
- [29] R. Wang, H. Feng, C. Huang, A New Mapped Weighted Essentially Non-oscillatory Method Using Rational Function, *J. Sci. Comput.* 67 (2016) 540–580.
- [30] P. Woodward, P. Colella, The numerical simulation of two-dimensional fluid flow with strong shocks, *J. Comput. Phys.* 54 (1984) 115–173.
- [31] R. Zhang, M. Zhang, C.W. Shu, On the Order of Accuracy and Numerical Performance of Two Classes of Finite Volume WENO Schemes, *Commun. Comput. Phys.* 9 (2011) 807–827.